

Delft University of Technology
Master of Science Thesis in Msc. Embedded Systems

An LC-to-Camera Communication System with Ambient Light

Rohan Katkam

An LC-to-Camera Communication System with Ambient Light

Master of Science Thesis in Msc. Embedded Systems

Networked Systems Group
Faculty of Electrical Engineering, Mathematics and Computer Science
Delft University of Technology
Mekelweg 4, 2628 CD Delft, The Netherlands

Rohan Katkam

10/03/2023

Author

Rohan Katkam

Title

An LC-to-Camera Communication System with Ambient Light

MSc Presentation Date

17/03/2023

Graduation Committee

dr. Marco Antonio Zúñiga Zamalloa Delft University of Technology

dr. Soham Chakraborty Delft University of Technology

Abstract

The current wireless networks can face congestion issues due to the increasing number of digital devices. One way to overcome this is to establish communication at a different range of frequencies, specifically in visible light. Most studies in Visible Light Communication (VLC) systems use active light sources like LEDs for transmission, but due to its high power consumption, studies have explored the domain of passive VLC that employs Liquid Crystal (LC)s. These systems utilize the existing lighting infrastructure, without needing dedicated LED transmitters. LCs modulate ambient light by controlling its polarization, thus encoding information. At the receiving end, a camera consisting of optical sensors captures and decodes these signals. However, single-pixel LC-to-Camera systems struggle to transmit data at high capacity. On the other hand, recent developments reveal that LCs can convert incoming light to polarized color signals under certain conditions. This thesis work exploits these properties to design a method that employs colors as data symbols in order to tackle the throughput issue. Therefore, we propose a multi-symbol, multi-channel LC-Camera system. We develop a modulation-demodulation mechanism that helps to establish a robust link. Experiments demonstrate an 8-symbol scheme results in a three-time throughput increase at per-pixel level with distances up to 160 cm at minimal error. We explore the scalability with a 2x2 pixel system that operates at rates four times that of a single pixel.

“The only thing greater than the power of the mind is the courage of the heart”
– John Forbes Nash Jr.

Preface

This thesis was selected due to my interest in seeking a research topic that combines communications and embedded systems. I was fascinated by the idea of using light for data transmission. Although there were initial hiccups in understanding passive-VLC systems, overall, it was an enriching experience. I'm thoroughly grateful to all those who were by my side during my journey.

I express my sincere gratitude to my supervisor Marco, for his continued guidance and support. His regular feedback helped me stay on track with my work. I also extend my thanks to Keyarash for his invaluable help and patience in clearing my doubts. I cannot thank my friends enough; they have been supportive and encouraging. I had a great time with my lovely buddies from numerous friend circles, notably, Toppers Group, My Dearest Hoes (MDH), Derry Cherry Gang, Leegh Bois, Vellegers of Bengland, and Nerd Herd. Working in the lab was a great experience, especially around jolly people, like Miguel, Mingkun, and Hao, and as well as other PhD and MSc. students. Lastly, I am indebted to my family for their love and affection.

Rohan Katkam

Delft, The Netherlands
10th March 2023

Contents

Preface	vii
1 Introduction	1
1.1 Problem Statement	2
1.2 Challenges	3
1.3 Contributions	3
1.4 Structure of the Report	4
2 Background	5
2.1 Polarization	5
2.2 Working of LC	5
2.3 Optical Response of LC	6
2.4 Voltage-Color Relationship	8
2.5 Color Representation	9
3 Related Work	11
3.1 Liquid Crystal as a Modulator	11
3.1.1 Single LC pixel	12
3.1.2 Multi-Pixels	13
3.2 Camera as Receiver	14
3.2.1 LED-Camera	14
3.2.2 Static Tags - Camera	15
3.2.3 An LC-Camera Setup	15
3.2.4 Work on Color Modulation Schemes	17
3.2.5 Work on Demodulation Scheme	17
4 Modulation	19
4.1 Passive CSK: A Prelude	19
4.1.1 Magnitude	20
4.1.2 Duration	20
4.2 LC Response	20
4.2.1 Theoretical Response	20
4.2.2 Voltage-to-Color Relationship	21
4.2.3 Color Intensities and Constellations	23
4.3 Timing Characteristics of LC	25
4.4 Symbol Selection	26
4.4.1 Algorithm	27
4.4.2 Types	28

4.4.3	Symbol Period and Channel Capacity	28
4.5	Multi-Pixel VLC	29
4.6	Packet Protocol Design	30
5	Demodulation	33
5.1	Capture and Extraction	33
5.1.1	Detection of ROI	34
5.2	Decoding	37
5.2.1	Decoding Algorithm Flow	37
5.2.2	Packet Detection	38
5.2.3	Preamble and Identifying Clusters	39
5.2.4	Payload Prediction	41
6	Testing and Analysis	45
6.1	Introduction	45
6.2	Setup	46
6.2.1	Transmitter Design	46
6.2.2	Receiver Design	47
6.3	Evaluation	47
6.3.1	Metric	47
6.3.2	Common Settings	47
6.3.3	Modulation Rate	48
6.3.4	Stack Size	48
6.3.5	CSK order	49
6.3.6	Distance	50
6.3.7	Lighting Conditions	51
6.3.8	Rotation	52
6.3.9	Pixel Count	52
7	Conclusion and Future Work	55
7.1	Conclusion	55
7.2	Future Work	56
7.2.1	Standalone System	56
7.2.2	Error Correction	56
7.2.3	Decoding Algorithm	56
7.2.4	Different LCs	57
7.2.5	High-end Smartphone	57
	List of Abbreviations	60

Chapter 1

Introduction

Wireless communication has existed for a long time and still has a large footprint in today's digital revolution. Most conventional wireless technologies lie in the RF frequency range, namely Bluetooth, WiFi, and cellular. Billions of devices are currently working over these networks, and the trend continues to increase at a staggering rate [27]. It will result in severe network congestion, and researchers have long been proposing to look for alternatives. The visible light spectrum (400-700 THz) is a good candidate as it lies in a different part of the EM spectrum. It's bandwidth is unlicensed and does not face interference from existing technologies. Light waves are used as a source and as a modulator to transmit messages. Furthermore, it does not pass through walls, so communication within a building is more secure as external parties cannot intercept it [31]. Thus, studies of VLC have increased in the last decade and have many applications, from indoor localization to sensing [48].

Typically, a VLC system uses LEDs to communicate with optical receivers such as a photodiode. LEDs are light-emitting diodes that can switch signals at frequencies compatible for the receiver to capture them. Such a VLC system where the light source is actively modulated with its intensity, frequency, is also termed "**Active-VLC**". While LEDs are universally present as illuminating devices, they function as VLC transmitters in many applications, from sending data in toys [7] to intelligent traffic control [33]. Active VLC achieves high data rates due to its ability to switch instantaneously between on-off states. This also ensures the flickering effects is not perceived by human eyes [30].

However, a major drawback with Active-VLC is that LEDs consume a significant amount of power to operate, typically a few watts [48]. In addition, it faces interference from surrounding ambient light. To overcome these challenges, researchers focused on saving energy by addressing two significant aspects:

- Instead of constructing light infrastructure for data transmission, use existing lighting in the environment.
- To this end, use energy-efficient devices that can modulate the light source to establish a communication link.

The points outlined above led to the emergence of the "**Passive-VLC**" domain which provides simpler and cost-effective solutions. This is because it does not require the additional cost in setting up a lighting infrastructure. The

communication channel relies on ambient light, for example, street lamps, indoor lights or even sunlight. Recent studies employed liquid crystals (LC) as ambient light modulators because they consume very little power, on the order of a few uWs [10], [16], [46]. They control the properties of incoming light waves, allowing them to block or let light pass through. This pattern of light and dark states can be used to encode data, and to achieve this, all we have to do is apply voltage across the crystal.

However, a single crystal needs at least one photodiode to receive stable signals. Moreover, to increase throughput, system can be scaled to contain multi-pixels, like a display screen [37]. In that case, an array of photodiodes would be required [41]. Fortunately, cameras are another option; they have a 2D grid of photo sensors built into them and can be used as a receiver in multichannel communication. More importantly, unlike photodiodes, they have a wide presence on smartphones and the number of phone users is expected to increase [29]. The camera chip contains millions of transistors and can function as VLC receivers. Each transistor is equipped with a red, green, or blue color filter, making it a color-sensitive device.

Although most ambient light studies have been over LC-to-photodiode systems [10, 3, 45, 41], only a few studies have investigated the combination of LC-to-Camera. They range based on the pixel size, viz. single pixel domain [47] or the multi-pixels domain [37]. They have data rates ranging from tens of bytes to a few kilobytes. However, LC-to-photodiode systems still perform faster on single-pixel basis.

Even so, most of the above mentioned passive-VLC systems relied on modulating with two states. More recently, *Chromalux* [10] expanded the design space for state selection. They examined a lesser-used optical property of crystals known as *birefringence*. In short, when light passes through LCs of a certain thickness, it generates a various colors as an output. This work can be translated to generate more than two distinct symbols, and theoretically improve the per-pixel rate. Therefore, we were motivated to develop a practical LC-to-Camera system that can increase the data speeds.

Additionally, we are inspired by the potential applications for passive VLC systems. Liquid crystals are manufactured and sandwiched between glass panels and are transparent in nature. Thus, we can convert windows in building spaces as passive VLC transmitters. Although some companies are working on the use of tinted glass panels for visual entertainment [39], s[43], we can imagine LC transmitters communicating the location of the building, maintenance, emergency details and other notifications. It can provide more accurate and up-to-date information about the environment. Smartphone users may scan a signboard of LC cells, where it captures dynamic data. We can visualize the deployment of the setup as illustrated in Figure 1.1.

1.1 Problem Statement

Thus, in our desire to fill the gaps in state-of-the-art systems, we strived to come up with a workable solution. For which we addressed the problem statement, and it boils down to the following question:

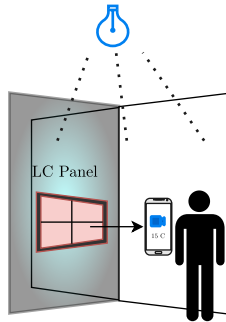


Figure 1.1: **Application of LC panel-to-Camera setup in indoor environment**

”How can we design an LC-to-camera setup for a passive-VLC communication, in which we can exploit the optical properties of a single pixel to maximize it’s throughput and also scale it to a multi-channel multi-pixel system?”

1.2 Challenges

For the purpose of this research work, we investigated the approach to key challenges.

- The main goal is to increase system throughput, but we need to confront the slow response times of the LC because it is a major bottleneck.
- In addition, the frame rate of a smartphone camera is low, making it difficult to capture faster changes on a transmitter. Thus, the sensor shall reliably notice the changes and extract the colors with good contrast.
- Given that the noise in the light channel can result in sampling errors and delayed bits, we need to develop a reliable decoding model.
- We need to create a system that can transmit multichannel symbols under varying lighting and distance conditions.
- Finally, we need to increase the LC pixels and simultaneously transmit symbols. The challenge includes the hardware control.

1.3 Contributions

We summarize the main contributions made during the research thesis as follows.

- We explored the voltage-color relation of the LC and explored it’s resulting color space. Then, we developed a Color Shift Keying (CSK) mechanism to modulate a single-pixel LC using colors.
- We designed a mechanism for symbol identification and selection that considers the LC response times.

- A passive VLC-compliant protocol was designed in which each packet is split between two segments. One segment contains information for synchronization and training sequence for demodulation. The second part contains the actual message or a payload.
- We developed an offline detection method to extract the color intensities as seen on the LC modulators.
- In addition, we came up with a decoding mechanism that includes packet detection, and a symbol training using k-means clustering algorithm. The resulting trained model is then used for decoding the received message.
- To test reliability, we evaluated the link under different lighting, distance, and orientation conditions.
- Also, we devised a Multiple-Input Multiple-Output system to maximize channel capacity. Here, we used a 2x2 grid of LC modulators as transmitters and a multi-sensor camera sensor as receiver. Our system is built on low-cost off-the-shelf components (COTS).

1.4 Structure of the Report

We categorize the report of our work into seven chapters. The second chapter introduces the background concepts relevant to the working domain, followed by a review of literary works. This is the third chapter that discusses the studies that constitute the basis of our research study. In chapter 4, we focus on the proposed modulation technique. After which, we detail the demodulation methodology at the receiver side. Then, we describe relevant experiments conducted, along with a discussion on their findings. Chapter 7 concludes by detailing the overall system flow, followed by mentioning the key results. It finally finishes with the suggestions for further research.

Chapter 2

Background

In this chapter, we take a look at the basics of optical properties of LC in passive-VLC. First, we explain how a liquid crystal can exploit polarization. Next, we introduce another critical optical phenomenon seen in LCs: birefringence. We examine how a configuration of birefringent LCs can help generate a spectrum of colors and explain how the colors are represented.

2.1 Polarization

Light consists of electromagnetic waves that travel perpendicular to the direction of propagation. Each light wave oscillates in a particular orientation, and in visible light *generally*, the constituent waves are aligned in random orientations. In this case, visible light is said to be "unpolarized". It is possible to filter out waves of a particular orientation through a process known as polarization. It is achieved by using a sheet of filter called a polarizer. We can see that in Figure 2.1, the polarizer allows only the waves oscillating in the vertical orientation to pass through. However, to exploit this property for passive VLC, we need to understand the functioning of LCs.

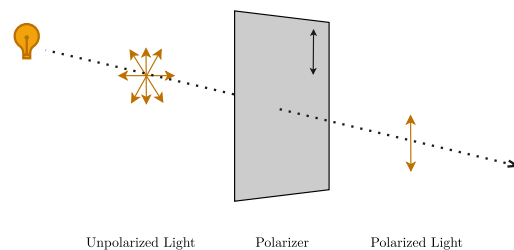


Figure 2.1: **Polarizer Working**

2.2 Working of LC

A liquid crystal is composed of tiny, transparent, rod-shaped structures that change their molecular orientation in response to an external voltage [36]. This

unique feature allows for LCs to change the polarization direction of incoming light. Importantly, LCs are used in conjunction with polarizers to regulating the intensity of ambient light. An LC is positioned between two polarizers, aligned orthogonal to each other and referred to as horizontal and vertical polarizers. We explain the operation with an example as shown in Figure Figure 2.2. The unpolarized light first passes through a vertical filter, where it gets polarized. When no voltage is applied to the liquid crystal, the polarized light rotates 90 degrees. As a result, the light has a horizontal orientation and aligns with the direction of the second polarizer. Thus, the light passes through, appearing transparent. We can assign this state to the binary "0". When the maximum voltage is applied, the LC molecules allow light to pass without twisting the polarization. This outgoing light is orthogonal to the second polarizer, hence is blocked. It creates an opaque state or represents a binary "1". It is worth mentioning that the transformation from unpolarized to polarized light reduces the intensity by half.

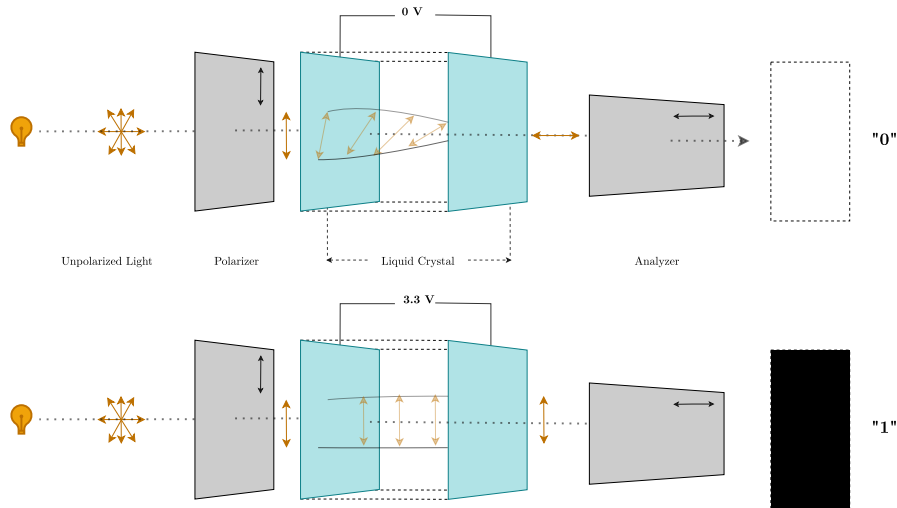


Figure 2.2: **Controlling Polarization using Liquid Crystals at two extreme voltages**

2.3 Optical Response of LC

Previously, the research in LC based illumination was limited only to binary states [8]. They employed techniques like On-Off Keying (OOK), where light signals represented a binary 1 or 0, similar to we saw in Figure 2.2. The LC's opacity was changed by switching between extreme voltage levels. Further, the researchers overlooked another reason causing transparency, which is an optical property called as birefringence. A study by Chromalux [10] revealed that by exploiting the changes in LC's birefringence, it is possible to visualize colors instead of grayscale. We need to understand the concept of birefringence before we can explain the implications of Chromalux's discovery for our research.

When a light ray passes through a transparent material like LC, its direction

and velocity changes. This measure of change is calculated by the refractive index of the ray. If the entering light is polarized, it splits into two separate rays at orthogonal orientations. This means that each polarization direction has a pair of different speeds, and different refractive indices. The faster one has an index of n_{max} , and the slower one is n_{min} . They leave the crystal with a phase difference between them, which can be measured by the difference in their indexes, also termed as birefringence. We can explain the property through an example illustrated in Figure 2.3. Birefringence is calculated as Δn in the equation below.

$$\Delta n = |n_{max} - n_{min}| \quad (2.1)$$

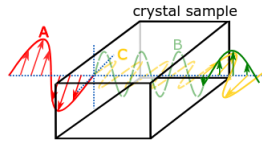


Figure 2.3: **Phenomena of Birefringence on an LC[10]. A single wavelength of red light upon incidence splits into rays of orthogonal polarization, where the green one travels faster in the LC more than the yellow wave.**

It is important to note that Equation 2.1 only applies to light containing one wavelength. However, white light is composed of a spectrum of colors at different wavelengths. When all these wavelengths exit the crystal, their polarization outputs merge, giving an impression of white light since human eyes cannot perceive polarization. Only after adding an analyzer, we can visualize those colors based on the polarization direction, as indicated in Figure 2.4.

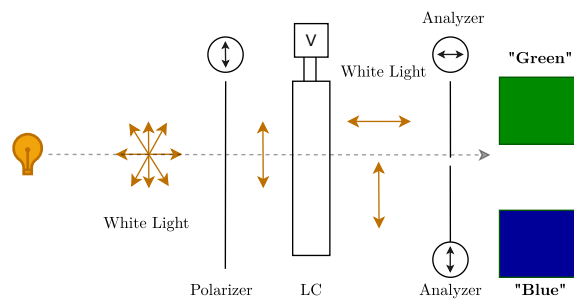


Figure 2.4: **Birefringence Output**

Additionally, the observed color at the analyzer is affected by the thickness of the crystal. The reason is that the thickness (t) impacts the separation between the orthogonal rays. This difference is known as the path difference, which is expressed in Equation 2.2. We use a Michel Levy chart to determine a certain color output based on the relationship between three factors: thickness, path

difference, and birefringence value. The chart is demonstrated in Figure 2.5.

$$\Gamma = t \cdot \Delta \quad (2.2)$$

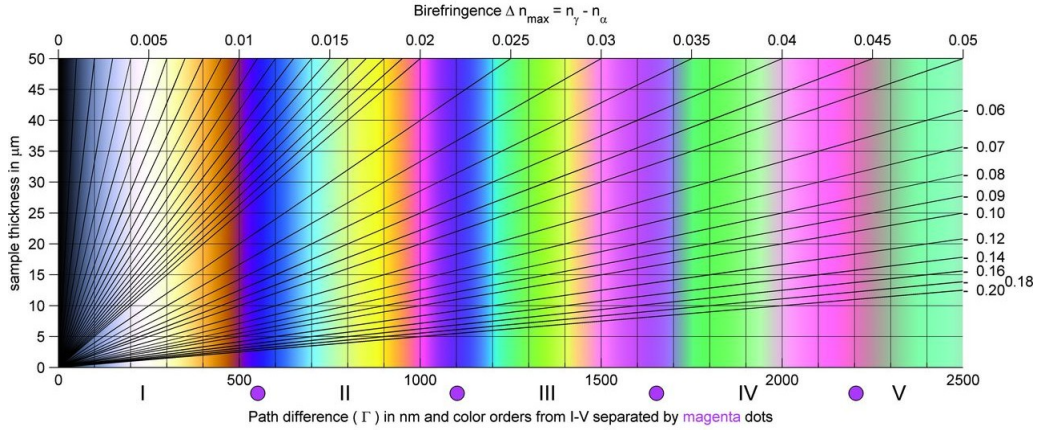


Figure 2.5: Michel Levy Chart [24] The order is defined as the path difference of 550 nm

The horizontal lines of the graph represent the thickness, the radial lines indicate the birefringence values, and the vertical lines shows the path difference. The intersection of these lines results in the color that is seen through the analyzer. It is important to observe that the we visualize a different color as we vary the path difference along the horizontal axes.

2.4 Voltage-Color Relationship

Interestingly, birefringence value can also change with voltage applied across the LC. When we apply a set of voltages anywhere between 0 and the maximum applicable voltage (V_{min} - V_{max}), we obtain a set of birefringence values. This translated into getting a color spectrum. The colors in this spectrum vary horizontally between two radial lines, one corresponding to V_{min} and one for V_{max} . We can see this relationship with the color output in the Michel-Levy chart illustrated in Figure 2.6a.

A typical thickness (t) of an LC layer for display applications is around 5 μm [21]. According to the Michel Levy color chart, this is represented as spectrum S_1 in Figure 2.6. This means, a single LC layer can only produce black-and-white displays, as the region between the radial lines falls on the left side of the chart. Thus, increasing material thickness is a likely option to produce colors. Instead, Chromalux's approach [10] involves grouping LCs together to emulate the working of a thicker LC. For example, stacking two LC layers increases the overall thickness (t) to 10 μm . The result is a shift of output spectrum along the same radial lines to the right with an increase in gap between them. Thus, we get a range of colors, as indicated as S_2 in Figure 2.6.

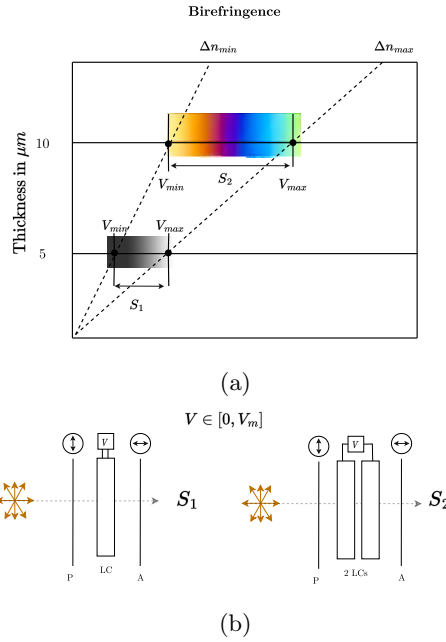


Figure 2.6: (a) Michel Levy chart indicating spectrum of two configurations: (b) single LC and 2 LCs stacked together

2.5 Color Representation

Our research is thus based on the aspects of birefringence, thickness and voltage response to generate a range of colors. It will improve the modulation capabilities of our system. Before selecting colors for encoding, we must quantify and organize them in a suitable color space. It is essential for our receiver to distinguish these values sufficiently to maintain a high Signal-to-Noise Ratio (SNR). That's why, we use a standardized color standard known as RGB space. It is a 3-dimensional space where the coordinates indicate the amounts of three shades: Red (R), Green (G), and Blue (B), required to match a particular color. It is illustrated in Figure 2.7.

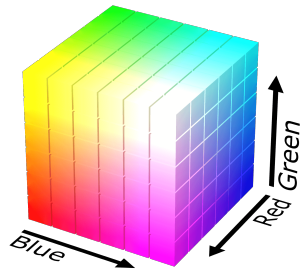


Figure 2.7: RGB Color Space [38]

The primary concept behind the transmission is that the LC modulates distinct data at specific voltage levels, which the camera sensor detects as colors. This produces a time-series response for three color channels, creating a multi-channel link. We can visualize the process in figure 2.8. In later chapters, we explore each segment of the communication in detail.

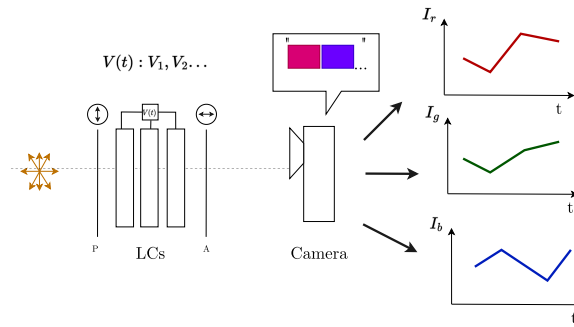


Figure 2.8: **System process**, I_r , I_g , I_b being the RGB intensities

Chapter 3

Related Work

In this chapter we examine previous research studies in passive-VLC domain. Unfortunately there are limited works regarding LC-to-Camera link. As a result, we investigate how the various components were employed in other studies. Specifically, we first review works that solely used LCs for transmission but a non-camera receiver. Next, we focus on systems that involve camera-based reception. We explain key insights and analysis that motivates our research. We highlight the the findings in a table. Next, we touch upon studies that used color schemes. Finally, we discuss the works where the decoding method was used. A summarized graph of the works are classified in figure 3.1.

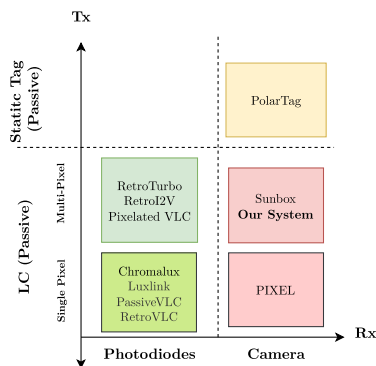


Figure 3.1: A Chart on Related Systems in Passive-VLC

3.1 Liquid Crystal as a Modulator

Most studies in this field have been conducted using LC to photodiode [41] setups, and as such we focus on how LC modulators are used in these systems. Photodiodes are susceptible to incoming light, so they tend to have a high SNR. They also have quick response times, allowing faster sampling rates compared to smartphone cameras. This section is divided on the basis of the number of LC pixels that are used as transmitters: single-pixel and multipixel. An LC *pixel* is defined as the smallest unit for display that modulates ambient light.

3.1.1 Single LC pixel

In this scenario, the transmitter can be a single LC or a group of LCs combined to form a unit with a surface area equivalent to a single LC. We examine systems that operate in natural sunlight, as seen in references [3] and [10]. There are also systems that rely on artificial lights, such as [41] and [16].

In **Luxlink** [3], the LC encodes binary data with Frequency Shift Keying (FSK) modulation. Compared to intensity-based OOK, FSK uses polarization to send a symbol, which means that opaque and transparent states alternate at different frequencies, making it robust. In addition, the system prevents modulation-induced flickering by shifting the analyzer to the receiver’s location, making the change in light signals undetectable along the Line-of-sight (LoS). This process, known as late polarization, is illustrated in Figure 3.3. The system can attain zero-error links at 80 bits per second and a range of 4 meters (indoor) and 60 meters (outdoor).

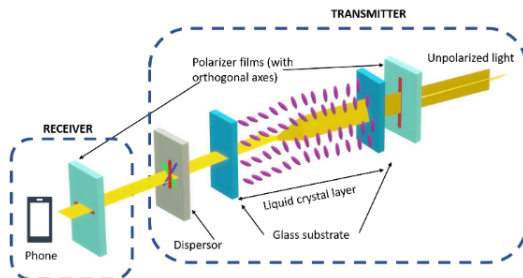


Figure 3.2: **Late Polarization** [3]

The study **Chromalux** [10], unlike previous single LC systems, stacks 4-6 LCs together. As explained earlier, this results in a broad color spectrum. However, they examined that certain regions within the spectrum produce non-linear transitions. It is possible to assign symbols close to each other in this region. It gives the system a high bandwidth and also increases the data rates. The ambient light was modulated and demodulated using a complex three-symbol state machine. The receiver identifies the signal’s variations and extracts the bits by comparing them against a set threshold. However, the transition region is unstable, making the receiver circuit. This is because it has to be tightly synchronized with the transition parts. Chromalux achieves a bit error rate of less than 1 percent at distances up to 50 meters, with a throughput of 1 kbps.

In contrast to Luxlink and Chromalux, where the receiver and transmitter operate in ambient light, PassiveVLC [46] and RetroVLC [16] use *retroreflectors* to reflect directed light to a modulator that is then sent back to the starting point of incidence, known as backscattering in VLC. The receiver is located at the light source in these systems.

In **RetroVLC** [16], the downlink uses narrow-beam LEDs that actively modulate light. The scattered light is modulated by a tag fitted with an LC shutter. The modulation is based on OOK, and to avoid a continuous pattern of the same symbol, they used *Manchester* encoding, sacrificing bandwidth at the cost data rate. The photodiode receives the modulated uplink signal and amplifies it. Then, a comparator detects these differences and decodes the data back to

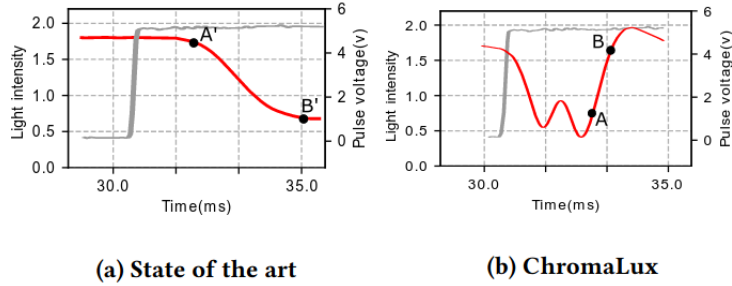


Figure 3.3: **Chromalux (b) has high bandwidth States assigned from the transient region compared to (a) [10]**

bits. The system achieved a maximum throughput of 500 bits per second in a range of 2.4 meters.

The setup of **PassiveVLC** [46] is similar to that of RetroVLC. However, it achieves higher throughput by employing the Miller coding scheme instead of Manchester coding. However, it is complex to implement and is susceptible to noise. PassiveVLC used an additional technique to boost data rates by reducing the switching interval between symbols. Rather than LC reaching a settled state, the incomplete transition was used to select states. The system throughput is at 1 kbps and was successfully demonstrated within the 2 m range. A PassiveVLC/RetroVLC system representation is illustrated in Figure 3.4.

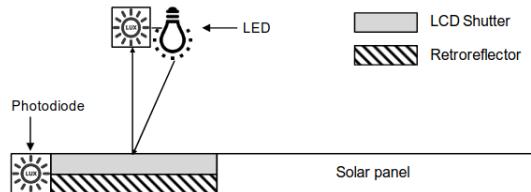


Figure 3.4: **Backscattering in RetroVLC/PassiveVLC [46]**

RetroVLC and PassiveVLC systems are considered semi-passive VLC systems because they use high-powered illuminators. However, their coverage areas are limited, as they have a narrow Field-of-View (FoV), which is also the case with Chromalux and Luxlink. Unlike PassiveVLC and Chromalux that employ transient areas, our system limitations restrict our focus on the settling states.

3.1.2 Multi-Pixels

In pursuit of maximization of the throughput in ambient light communication, some studies came up with a pattern of connected LCs. Multiple shutters modulate simultaneously, creating parallel links and linearly scaling up the data rates. We examine the works of **RetroTurbo** [41] and **RetroI2V** [40]. These systems are multiple-input and multiple-output (MIMO), in which the LC-shutters function as transmitting antennas and photodiodes as receiving antennas.

In **RetroTurbo** [41], the transmitter consists of 64 LC shutters divided into groups of 4. To efficiently modulate all of them simultaneously, they devised two schemes: *Delayed Superimposition Modulation* (DSM) and *Polarization-based Quadrature Array Modulation* (PQAM). In DSM, a symbol is created by adding the intensities of LCs within a group. It ensures the symbol duration accounts for all of shutter’s response times. Additionally, P-QAM uses a combination of Quadrature amplitude modulation (QAM) modulation and polarization to achieve multiple states. The photodiodes are equipped with two analyzers aligned at 45 degrees angles, resulting in two independent channels. Through these methods, the total system symbol count increases to 256. An offline regression algorithm predicts the data with known model coefficients. The model was trained with a large set of ideal signals. Here ideal signal means that the waveforms were transmitted from each LCM under optimal brightness conditions. The overall system capacity runs at 4 kbps at a distance of 7.5 m with a Bit Error Rate (BER) of $< 1\%$.

RetroI2V [40] employed a large grid of 6x6 LC shutters that modulates light using OOK. Unlike Retroturbo, this setup employs a complex channel estimation model to account for channel errors. Additionally, a *linear regression* algorithm is used to recover the components of the signal. The results of their experiments show that RetroI2V can work at large FoVs (at $\pm 18^\circ$) with a $< 1\%$ BER at a rate of 1 kbps and an impressive range of 80 m.

Pixelated-VLC is [34] is an improvement over RetroVLC [16] in terms of increased channel throughput. The system has an array of LC shutters modulating with Pulse Amplitude Modulation (PAM). For example, each pixel produces two level outputs, and combining three pixels allows eight different pulses to be generated. Therefore, the throughput is three times greater than that of a single pixel. The data rate is 600 bps for a distance of 10 meters.

Like single-pixel backscattering systems, both RetroTurbo and RetroI2V have a drawback of high power consumption, with lamps consuming between 3 to 30 W. The LCs in these systems respond slowly to voltage changes, which is a bottleneck for passive VLC-based links. Furthermore, they only considered a limited design space for symbol selection, and thus chose only two levels per LC pixel.

3.2 Camera as Receiver

In contrast to the backscattering systems mentioned earlier, which employed photodiodes with a limited field of view, a camera receiver provides a wider field of view for data collection. The camera is equipped with photosensors that can receive multiple data streams transmitted by multiple VLC transmitters. In this way, they create single-input and multiple-output (SIMO)/MIMO links, providing reliability and ease of deployment. We divide this section by the type of transmitter used: LED, static tags, and LCs.

3.2.1 LED-Camera

Studies on LED-camera captured the incoming light as videos [28], [4]. The data was modulated based on the intensity of the LEDs. However, the speed at which the LEDs switch is often much faster than the camera’s sampling speed.

To overcome this, the rolling shutter is used to allow the camera to capture light for a longer period of time, thereby capturing more information while still maintaining a high LED switching frequency. Studies like [11] used a rolling shutter to increase data transmission rates by sending 8 symbols using color LEDs for indoor localization.

In **POLI** [5], birefringent dispersers split the LED light into color beams, which are then filtered through a polarizer and perceived by a camera as RGB signals, as shown in Figure 3.5. It proposed a polarized-based intensity modulation (P-CIM) scheme in which color symbols are mapped to the intensity values of LEDs. The modulated signals from the LEDs are polarized in distinct orientations. However, the intensity of transmitted light is maintained at a fixed level because the signals are aggregated with a beam combiner. The decoding scheme uses *bilinear interpolation* and compares the incoming color signals with a lookup table. The table stores the intensities of the known training symbols sent at the beginning of packet transmission. With three high-power LEDs, 16 symbols are used for modulation, resulting in a data rate of 72 bps in a range of 10 m.

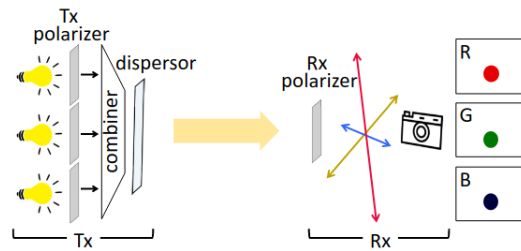


Figure 3.5: **POLI's setup, polarized light from three LEDs into separate beams of different colors**

3.2.2 Static Tags - Camera

Polartag, like POLI, utilizes optical materials to produce birefringence. However, it polarizes ambient light using static tags rather than an electrically controlled liquid crystal. The tags contain reference and payload cells. The Polartag camera receiver recognizes colors by examining the polarization at different angles. The captured color values are compared to the reference cells during decoding and thresholded into binary data. Polartag has a field of view (FoV) of 110 degrees, making it suitable for non-line-of-sight positioning with a range of 3 meters and a zero-bit error rate, with a system rate of 40 bits per second. The use of static tags eliminates the issue of LC's transition times. However, given that the content of the cells is fixed, they cannot transmit continuous dynamic data.

3.2.3 An LC-Camera Setup

Here, we look at related studies that form the basis of our setup. LC-Camera in passive VLC has only been conducted by a single LC pixel like the work done at PIXEL [47] and the multi-pixel that was conducted by Sunbox [37].

The first LC-Camera study to use ambient light is **PIXEL** [47]. It was devised for indoor positioning using ceiling lamps as a light source. The modulators are directly attached to the lamp for maximum light availability and stable link. Similar to Luxlink [3], the analyzer was placed next to the receiver. Most studies with LC use polarization to encode binary states. However, it is not robust to rotations between the transmitter and receiver, causing rapid degradation in signal transmission. This is illustrated in Figure 3.6. To address this problem, PIXEL added dispersors, similar to what we noticed in POLI. This way, a color spectrum is produced. To this end, the encoding utilizes *Binary Color Shift Keying (BCSK)*.

They utilized BCSK which encodes binary states as two distinct colors. This is designed in such a way that the camera receives two distinct colors irrespective of the analyzer's orientation. Due to their uneven sampling in the camera, PIXEL devised an algorithm that uses OS clocks to sample the data more evenly. The points are downsampled based on their highest SNR. The selected points are compared with a threshold reading to decode it to 0 or 1. The transmission rates was 14 bps at a distance of 10 m.

The approach of obtaining color in the VLC link by PIXEL differs from Chromalux [10]. The net thickness of the modulator in Chromalux was higher than that in PIXEL and gave a more extensive color range. PIXEL, on the other hand, relied on an LC-dispersor combination. Unlike Chromalux, they do not use intermediate voltages, nor employed multi-symbols.

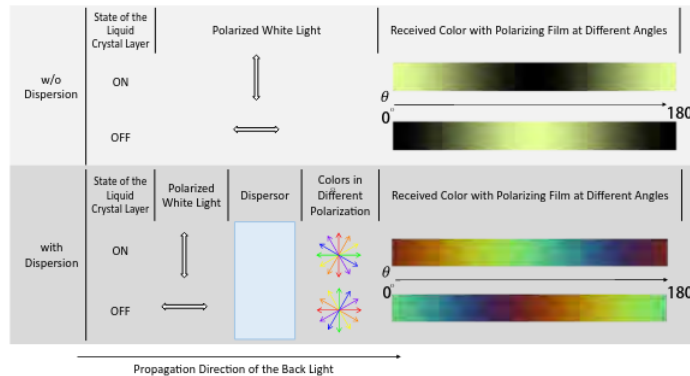


Figure 3.6: **BCSK in PIXEL; when the angle is 0° , an orange is "1" and a turquoise represents a "0"**

Since PIXEL worked only with one-pixel modulators, **Sunbox** [37] is the first passive VLC screen-to-camera system. The screen is a microdisplay made up of smectic LC pixels that modulate the natural light with black-white states. They are expensive to manufacture, making them cost-ineffective. However, smectic LCs have to switch responses faster than those nematic LCs. Sunbox does not utilize a modulation scheme. Instead, the data is represented as a series of QR codes. A low-end smartphone camera records the patterns on the screen as frames. The data is decoded with existing extraction methods used for QR. The transmission rate was 20 QR codes per second and the receiver sampled 30 frames-per-second (fps). Although the camera has problems capturing at that

System	Transmitter/Modulator	Receiver	Tx Pixel Count	Symbols per pixel	Bit rate
PassiveVLC	LC	Photodiode	1	2	1 kbps
RetroVLC	LED and LC	Photodiode	1	2	0.5 kbps
Pixelated-VLC	LED and LC	Photodiode	1	8	0.6 kbps
Retro2V	LED and LC	photodiode	1	2	1 kbps
RetroTurbo	LED and LC	Photodiode	64	2	8 kbps
Luxlink	LC	Photodiode	1	2	80
Chromalux	LC	Color Sensor	4-6	3	1 k
Sunbox	LC	Camera	720x540	2	10 kbps
Polartag	Static Tags	Camera	24	4	40
PIXEL	LC	Camera	1	2	14

Table 3.1: Summary of the State-of-the-art

transmission speed, packet losses are compensated with Reed–Solomon (RS) error correction method. Sunbox achieved a total throughput of up to 10 kbps, but the system was unable to work beyond 10 cm due to the display size.

An overview of relevant studies is presented in tabular form in Table 3.1.

3.2.4 Work on Color Modulation Schemes

Color modulation methods were used to encapsulate more information than traditional on-off techniques. It was in the active VLC domain [44] [13]. Fast-switching RGB LEDs can produce a wide range of distinct colors, and a higher number of different colors leads to higher throughput. A study [23] proposed CSK that uses different colors of LEDs to represent different symbols. Another study focused on Color Sequence Shift Keying (CSSK) [22] that uses a sequence of colors as a symbol. In CSSK, the color changes, but the light intensities of the LEDs remain constant. In passive-VLC, only PIXEL and Polartag have worked with color components for information encoding. There have been no studies on LC-camera systems using higher-order color modulation methods beyond binary color modulation schemes.

3.2.5 Work on Demodulation Scheme

Machine learning (ML) techniques have been applied in various research fields, including active-VLC. They improved decoding accuracy while compensating for channel interference problems [19] [18]. Smartphone cameras are frequently used in ML applications, for purposes such as classification, tracking, and segmentation of objects [42]. The work at [12] used a camera to record data from LED panels and decode the camera data using *regression* models. The combination of camera and ML can capture visual information and identify patterns, rather than relying on complex signal processing methods [5, 46] or state machines [49]. However, to the best of our knowledge, there has been no use of a camera as a receiver in passive-VLC using supervised, semi-supervised or unsupervised ML.

Chapter 4

Modulation

As discussed in the previous chapter, most research on passive VLC relied on LC's transparent and opaque conditions for transmission. These LC states will modulate the polarized ambient light using binary schemes like OOK or FSK. The modulation data will be decoded on the basis of their perceived intensities at the receiver. Thus, LC-to-camera systems were limited only to these binary-based modulation methods, which limited their per-pixel data rate. Our research work focused on finding methods to address the low-throughput problem. LCs, through birefringence, can produce a color spectrum [10], and our research goal translated this idea into a high-throughput modulation scheme, which was not explored for LC-Camera links before. The communication method, also known as **CSK**, involves using the magnitude of colors as transmission symbols. A multi-symbol communication link is established, allowing more data to be encoded than just binary states.

Our work to maximize the data rate is focused on the modulation of a single pixel. We first introduce the CSK scheme and how it is expected to take shape. To develop the modulation method, we need to understand the factors that affect its design. It requires a discussion of its symbols. A CSK symbol is affected by two factors: its magnitude and duration. The magnitude section is established by selecting colors. Therefore, we first understand how LCs theoretically and empirically produce colors. We talk about its representation through constellation diagrams which lay the footwork for selecting favorable CSK symbols. To examine the symbol duration, we analyze the timing characteristics of LCs. Next, we discuss the mathematical formulation for mapping color intensities as CSK symbols. We discuss how our modulation can be optimized through a section on channel capacity. Next, we detail how multipixels can create multiple pathways for faster data transmission. Finally, we use a protocol design approach to systematically translate digital bits into polarized light signals for reliable transmission.

4.1 Passive CSK: A Prelude

The polarized ambient light goes through birefringent LCs to give colors. CSK modulation aims to use these colors as symbols for VLC transmission effectively. It is an intensity-based color keying scheme similar to those utilized in [23] and

[5]. A symbol uniquely designates the digital data, and we map each symbol to a color. Using a larger set of distinct colors, we can encode more information, which in turn increases the data rate of the communication link. For example, a CSK symbol can represent data "000," which has the capacity to transmit data three times more than a binary bit '0'. Two primary factors that influence the design of a symbol are **magnitude** and **period**.

4.1.1 Magnitude

The magnitude of these symbols affects the **SNR** of the communication link. The color symbol is split as intensities along RGB values. The receiver perceives these values with a particular contrast. Higher contrast means that the receiver can better differentiate between different colors and recover the transmitted information more accurately.

4.1.2 Duration

We communicate each symbol with a sufficient duration known as the symbol period. It directly affects the maximum rate of symbols that can be transmitted. The symbol rate (S) can be calculated as the inverse of the period (T), with a higher rate indicating a faster transmission speed. We describe it as follows.

$$S = \frac{1}{T} \quad (4.1)$$

However, achieving this reduction depends on accounting for the following considerations:

- Slow Response Duration: LC, due to its material properties, does not respond or produce output instantaneously.
- Receiver's sampling time: that refers to the duration required for the receiver to capture and receive an intensity, allowing for error-free decoding.

The longer the symbol duration, the lower the transmission data rate, but if its symbol period is short, then it can cause Intersymbol interference (ISI) in the channel, that is, distance between the symbols in the constellation is reduced. Our initial approach is to analyze the colored output of LC theoretically. This is followed by an empirical translation of voltage to color to obtain contrasting colors.

4.2 LC Response

4.2.1 Theoretical Response

We have discussed earlier that the polarized light from a liquid crystal generates an output that is visualized from the Michel Levy graph in Figure 2.5. However, to understand how the colors in the chart are mathematically realized, we have to understand LC's theoretical response. It is based on the following equation:

$$L = \sin^2\left(\frac{\pi \cdot \Gamma}{\lambda}\right) \quad (4.2)$$

Here, L refers to the fraction of light transmitted of a wavelength (λ) after exiting the analyzer. Γ is the liquid crystal's path difference. It is important to note that this equation applies to a single wavelength. We are working with an ambient light spectrum, so we have to sum the results for all its constituent wavelengths. After this summation, we get a transmission matrix for each color in the graph [35]. We aim to produce an **RGB** representation from the matrix, since it is a supported color space format for the camera hardware. Therefore, we use color matching functions for this transformation procedure, which [6] convert the amount of light resulting from a color to a 3-dimensional vector $[X, Y, Z]$. This vector corresponds to transformed data from three channels: Red (R), Green (G), Blue (B), respectively. We can denote it by L_{XYZ} shown in Equation 4.3

$$L_{XYZ} = \begin{bmatrix} X \\ Y \\ Z \end{bmatrix} \quad (4.3)$$

L_{XYZ} gives us a vector value for a single color of a specific path difference (Γ). By varying Γ from 0 to 2500 nm, we get a numerical response that describes the Michel Levy chart colors appearing on the liquid crystal. The vector variation with the path difference is illustrated in Figure 4.1. The graph Figure 4.1 is produced through a set of equations discussed in Chromalux [10] and [20].

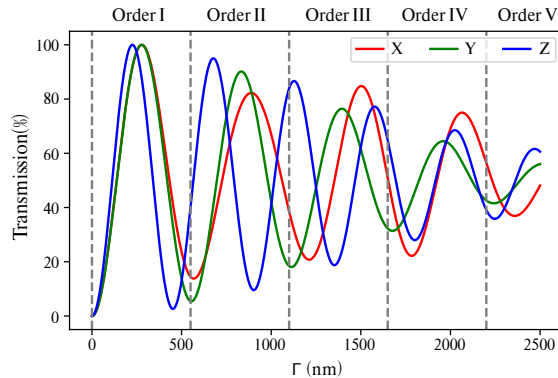


Figure 4.1: **Decomposed Color Response** [10]

In the first order, all the channel magnitudes begin from zero, indicating black color, rise in unison, and reach the first peak, white. The behavior is monotonic and in phase. As the order increases, the values go out of phase, resulting in color.

4.2.2 Voltage-to-Color Relationship

In practice, the visual outcome of LC only covers a portion of the theoretical graph. The colors obtained are affected by changing two parameters, thickness and voltage. As the thickness of the LC increases, the value of the path difference also increases, causing the response region to shift to the right as shown in Figure 4.1. Within this region, the intensity of X, Y, and Z can be influenced

by adjusting the voltage value. However, since the birefringence values of the LC are unknown, it is difficult to determine the exact correspondence between the voltage-thickness combination and the theoretical XYZ values. Also, the intensities can differ from the receiver's output. So, to further explore these trends empirically, we conducted an experiment as follows.

We use indoor ceiling lights as an illumination source. We change the voltage in a single LC from 0 to 3.3 V, with a step size of 0.1 V. This gives us 34 voltage points/levels. A camera receiver takes pictures of the resulting color output of the transmitter. The images will be processed to extract the RGB data. The procedure is repeated for a stack of 2 to 4 LCs. The experimental responses are normalized from (0-255) to (0-1) and plotted as colored charts in Figure 4.2 and as channel magnitude plots in Figure 4.3.

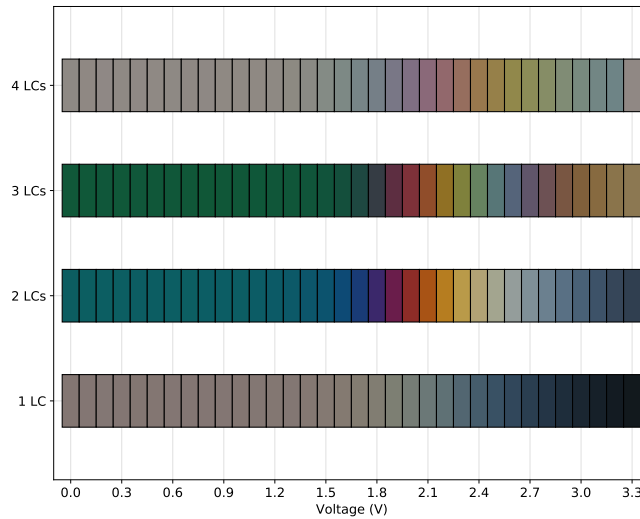


Figure 4.2: **Color Spectrum at the camera based on voltage levels across the LC stack**

Analysis of the Responses

As depicted in Figure 4.2, there is a common trend across all stack sizes, i.e., there are no color transitions below 1.8 volts. It is caused by the inability of LC molecules to change polarization. This minimum operating voltage is referred to as the Fréedericksz threshold [10].

In Figure 4.3, it is essential to note that the experimental and theoretical measurements are mismatched because, in XYZ, each channel has a different range of values, whereas the RGB channel follows an equal range (0-255) [10].

The channel intensities of 1 LC as depicted in Figure 4.3 indicate a response similar to the rising edge of the first order in Figure 4.1. Additionally, the spectrum covers a grayscale region similar to that seen in Figure 2.5. Most

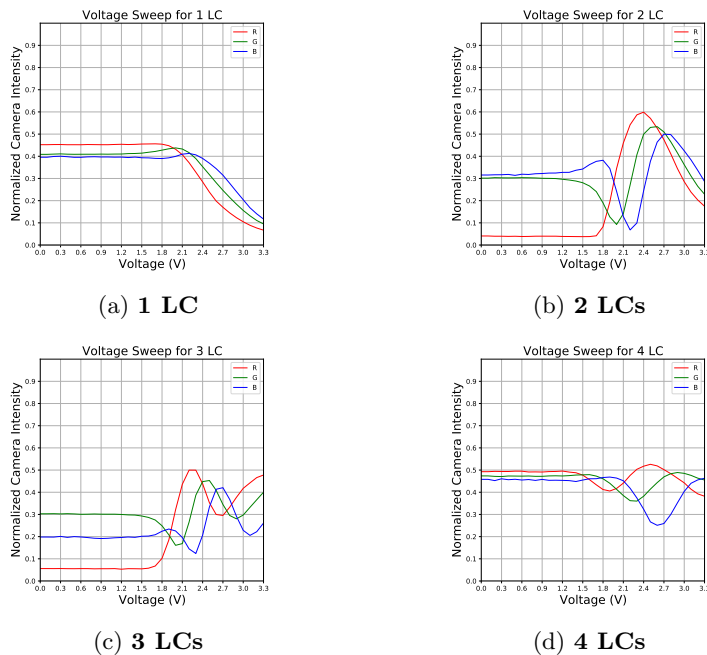


Figure 4.3: **Response of the camera according to the size of the stack. The LC pixel value is represented as a tuple of 3 color channels, each with a normalized intensity.**

passive-VLC research focused on this region; therefore, they could utilize only transparent and opaque states for data transfer.

More than one LCs in a stack create a non-linear color spectrum response. The RGB curves in a 2 LC stack traverse from first to the second order in Figure 4.1. As we continue to add more LCs, the order number increases. The channels go more out of sync, resulting in a dynamic range of colors as seen in Figure 4.2. In addition, the colors corresponding to this range are shifted to the right in the Michel Levy chart (Figure 2.5).

Importantly, we notice that the stack size is inversely proportional to the contrast of the RGB channels. Upon closer look at the spectrum responses in Figure 4.2, appears less bright in comparison. Similarly, the peak magnitudes depicted in Figure 4.3 are highest for a 2 LC transmitter (with peaks ranging between 0.5 and 0.6). This trend is also evident in the theoretical response shown in Figure 4.1. The cost of going to higher order reduces the channel amplitudes, leading to lower contrast.

We aim to have color signals with a high SNR. This means that the contrast must be high and thus, comparing to camera responses of different LC-sizes, we choose a 2 LC stack as the modulator.

4.2.3 Color Intensities and Constellations

To visualize the voltage-color response spatially, use a constellation diagram. It assists in identifying the colors that can be candidates for potential CSK-

states. We consider the measurements for the voltage range of 1.8 to 3.3 V. These intensities are plotted on a 3D graph along the RGB coordinate axes. It is shown in Figure 4.4. Each such value is considered a constellation point on the constellation graph. Let C_p describe the vector of a constellation point produced at p Volts and be given as:

$$C_p = \begin{pmatrix} r_p \\ g_p \\ b_p \end{pmatrix}$$

r_p , g_p , and b_p are the normalized RGB magnitudes. We can see in Figure 4.4 that the points are arranged along an oval-shaped curve-like pattern known as a constellation curve.

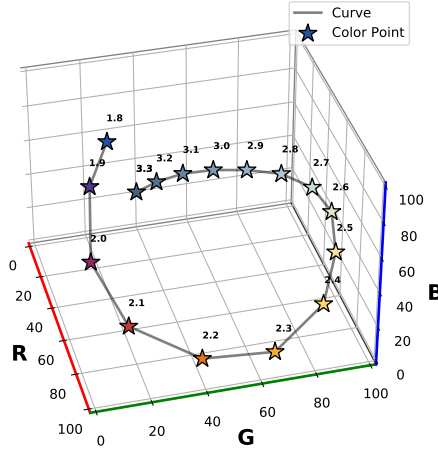


Figure 4.4: **3D Constellation graph for 2 LCs at a voltage range of 1.8 to 3.3 V, the points depict it's corresponding output color**

Next, we look at how to consider far-apart points to maximize SNR. Otherwise, selecting close points will be heavily affected by the noise in the light channel, resulting in a low contrast. We choose the Euclidean distance metric to measure this closeness. Consider two points of voltage i and j ; the distance is calculated in 4.4. If the distance is below a predetermined distance threshold ($T_d = 25$), we say that the two colors are *similar*. Otherwise, the colors are said to be *contrasting*. We notice that the colors within 3.1-3.3 V are similar. In this case, the colors of the LC pixel are very close to dark-gray values as seen in Figure 4.2.

$$\begin{aligned} d_{i,j} &= \|C_j - C_i\| \\ &= \sqrt{(r_i - r_j)^2 + (g_i - g_j)^2 + (b_i - b_j)^2} \end{aligned} \quad (4.4)$$

However, the constellations do not provide a complete picture for the selection of symbols. The graph does not indicate the response time to change between color points; this is important because it impacts the CSK-symbol period. So, in the next section, we talk about how the LC's timing response affects output colors' generation.

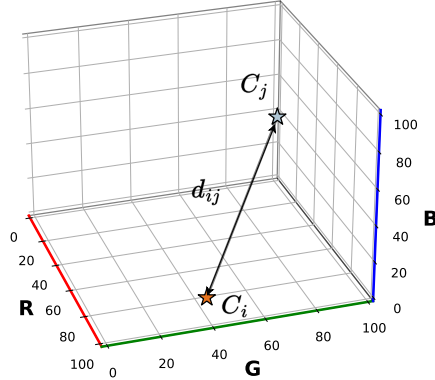


Figure 4.5: Distance between two constellation points

4.3 Timing Characteristics of LC

In reality, the LCs do not instantaneously toggle between two voltage levels. This happens because the LC molecules take time to orient to a new configuration. From a receiver’s perspective, it will notice a transitional change from one state’s magnitude to another. In other words, the camera notices the change in intensity in a color channel. There are two types of durations for a pair of voltage levels: the rise time and the fall time. We can understand this with an example illustrated in Figure 4.6. The rise time is the change from 2.2 to 2.8 V, and the fall is vice versa.

We aim to estimate the duration of the transition so that the symbol period can account for these changes. Otherwise, the receiver cannot confidently decode the correct symbol by looking at the transient region. It is essential to wait for the state to settle to its expected color magnitude. Therefore, we conducted this estimation study using a photodiode as receiver; it has a faster sampling rate than a smartphone [37] and records transitional trends on a finer scale. Individual RGB filters were placed to record the intensity of channels separately; these color filters allow light from a particular color to pass through [1]. The noisy samples were filtered from measured data through convolution. Eventually, we get the voltage toggle shown in Figure 4.6. To distinguish the transient region from the settled ones, we calculated the gradient of the data and compared it with a predetermined threshold ($T_g = 0.1$). Any data points above this threshold were identified as within the transition region.

Transition times Experiment

We repeat the experiment mentioned above to accurately calculate the response times for all possible voltage combinations (within 1.8 and 3.3 V). We compile a table of all rise and fall times based on these findings, which is illustrated as a heatmap in Figure 4.7.

We notice that the fall times are higher than the rising times. Chromalux [10] argued that the reason behind this is due to the capacitive behavior of LCs. The

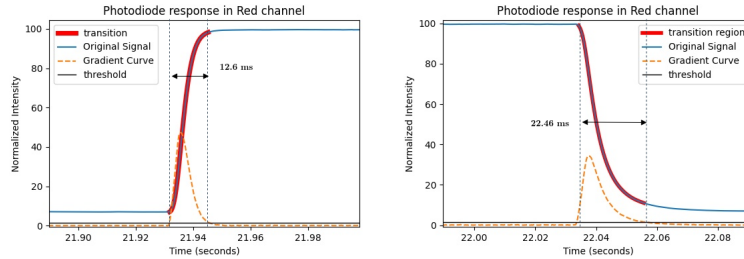


Figure 4.6: **Rise and fall times, the rise time in this case is for switching between 2.2 and 2.8 V**

heatmap in the bottom left is bright due to slow fall times between significant voltage differences. They have longer falls because of the large voltage gap, so this is a bottleneck to our symbol design. The maximum transition time in this region is 24.8 ms, but it contains voltage points that generate distinct colors. To ensure a high signal-to-noise ratio (SNR) and maximize the number of CSK symbols, symbols chosen for this region must have durations that exceed the maximum response time.

The bottom-right region of the heatmap includes low response times (≤ 9 ms). The states here almost plateau to the final stage of LC, after which the molecules do not rotate any further. We cannot assign symbols solely from this part because it does not favor our receiving system. The camera has a maximum capture rate of 120 fps, so using Equation 4.1, the sampling period is 8.33ms, which has a bandwidth not sufficient to capture some of the settled states, causing detection errors. More importantly, the colors here are similar, making it harder to detect distinct intensities.

4.4 Symbol Selection

Considering the bottlenecks mentioned above regarding the response times and the camera's sampling speed, we resolved to design a high throughput and error-free CSK scheme by targeting two fronts:

- We maximize the number of contrasting colors to maximize the number of symbols. Increasing the contrast between colors is more likely to result in a significant improvement in SNR.
- For the chosen symbols, minimize the symbol period. It must not be shorter than transition times because the backflow effect might result in unstable predictions [10]. Thus, we include an additional duration for settling time so that the camera can capture the change in encoded signals.

The camera sensor does not necessarily need to detect incoming RGB colors with the same magnitudes as the original transmission. However, if the symbols are widely spaced, the decoder can easily distinguish between them. When the points in the color space are closer together, the colors are considered to be more similar. Therefore, we developed a symbol selection algorithm that identifies the group of constellation points that are maximally distant from each other.

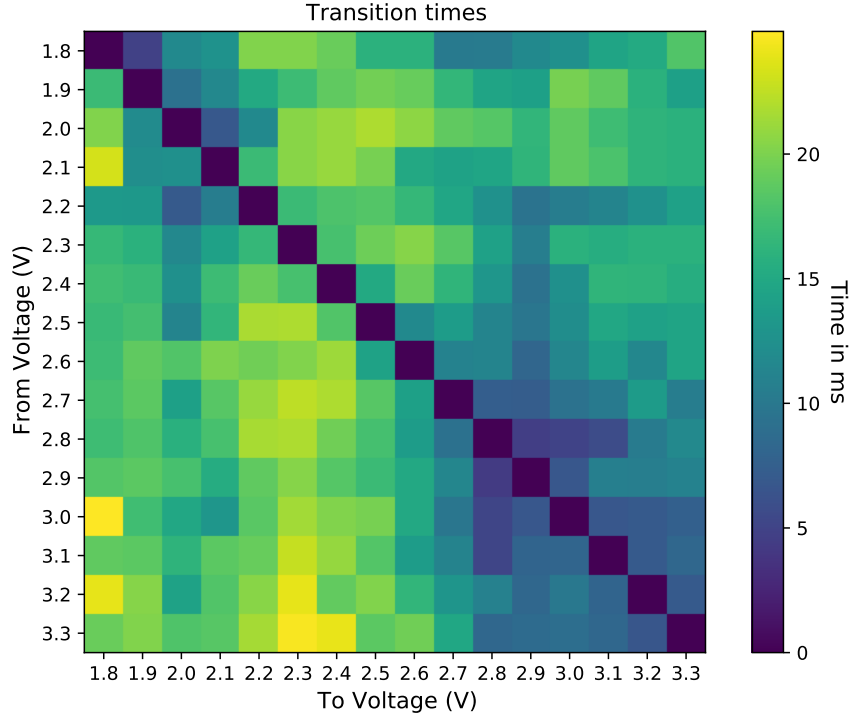


Figure 4.7: **Heatmap of Transition Times**

4.4.1 Algorithm

The algorithm aims to optimize the selection of N symbols for CSK by maximizing the minimum distance between them. We choose a subset k of size N from the set of constellation points of size \mathbb{P} to achieve this. Then we determine the distance between each pair of unique points (i and j) within k , and from this we keep track of the minimum distance $d_{min,ij}$. Here, the distance is the intensity different calculated using Equation 4.4. We repeat this process for all possible combinations of size N to obtain a list of minimum distances. A linear search is performed to find the maximum from the list of these minimum distances. A mandatory criterion for the objective is that the distance between two points in the subset must be greater than a predetermined contrast threshold (T_d). The algorithm reaches its solution by obtaining the group of points that contains the max-min distance and is denoted as S_k in the equation 4.5. It is important to note that each constellation point corresponds to a voltage level as illustrated from Figure 4.4.

$$S_k = \arg \max_{k \in \mathbb{P}} \min_{i,j \in k} d_{i,j} \quad , \text{ if } i \neq j, d_{i,j} > T_d \quad (4.5)$$

4.4.2 Types

We define *order* of passive-CSK as the number of distinct symbols used for transmission. From the subset obtained in Equation 4.5, we get N -voltage levels for an N -CSK scheme. For instance, 4-CSK indicates that we employ four symbols, each containing two binary bits. The symbols are thus represented in the format shown:

'A' (1.9 V): '00', 'B' (2.2 V) : '01', 'C' (2.4 V) : '10', 'D' (2.9 V): '11'

Generally, the number of bits in a symbol is calculated as $\log_2 K$, where K is the number of different colors. The constellations for 4-CSK and 8-CSK are visualized in Figure 4.8. Based on the algorithm and the criterion, we can, in principle, expect a CSK order of up to 10 unique points. Next, we determine the duration required to transmit the symbols.

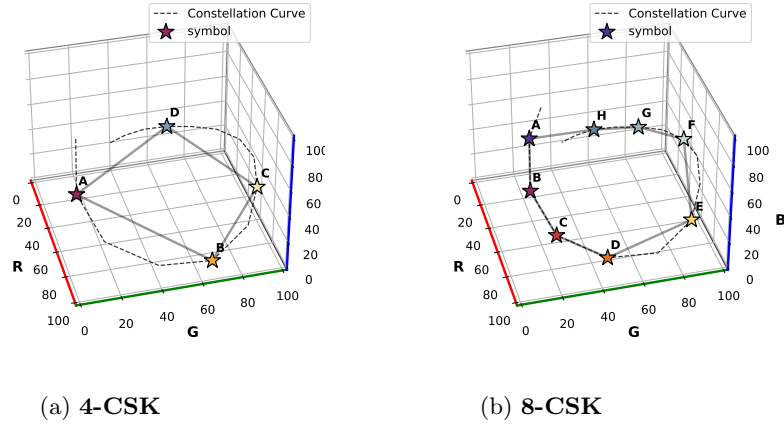


Figure 4.8: CSK Types

4.4.3 Symbol Period and Channel Capacity

The passive-CSK scheme not only selects the farthest constellation points in space but applies a long enough symbol duration time to let the intensities reach their settled states. We emphasize the settled region because the camera will reliably demodulate signals based on constant intensities of colors. It is also important to note that the period is maintained equal for all symbols, making our decoding easier. The symbol interval accounts for the worst possible rise or fall transition scenario. For example, in 4-CSK, the longest switching time of 22.6 ms occurs between 1.9 and 2.9 V; this implies that we fix a symbol duration to be greater than this value. Additionally, an extra duration is added to the total symbol interval to give sufficient time to transmit settled regions. To this end, we calculate the state duration and the resulting data rate by looking at the longest duration for a CSK.

For contrasting color set for 8 or 10 CSK, longest duration is **24.8 ms**, and for 4-CSK it is **22.6 ms**. We denote this as the transition time t_{tr} after which

we allocate time for settled duration, known as t_{st} . The period of the symbol is thus t_s given as:

$$t_s = t_{tr} + t_{st} \quad (4.6)$$

To maximize the rate, we have to minimize t_s , but the only tweaking parameter is t_{st} . The worst possible transition time is set to 24.8 ms. We must consider the Nyquist criterion for the reception to adjust the settled time. Under the sampling theorem, the camera sampling rate must be twice or more than the transmission rate to extract data signals reliably. The camera captures the signals as a series of frames. In other words, we must set the symbol period where at least two frames can capture a transmitted symbol. Another criterion is that the decoding algorithm requires more than one frame corresponding to the settled intensities. However, this comes at the cost of considering frames corresponding to the transient region. To explain clearly with the worst case scenario, each frame is sampled at every 8.333 ms. When two frames are captured, the symbol period is still at the transient stage of 24.8 ms. Once the transitions plateau to the stable part, the camera samples the third frame at 25 ms. This is registered as the first settled frame. To satisfy our receiver conditions, we also record the next instance of the frame, which occurs at 33.33 ms. Thus in total, when we capture four frames across a single stat, in the worst case, we get two frames for transient and two for settled.

Any duration greater than 33.33 ms will result in the capture of more than four frames per symbol. This means that the transmission rate drops. Thus, the minimum symbol duration is 33.33 ms. Using 4.1, the maximum throughput for our LC-camera link that we can achieve is 30 Ssec^{-1} (Symbols per second). Since our system works with binary data, we measure the capacity of data transfer in the network using bits per second, which is formulated as B as mentioned below:

$$B = S \cdot \log_2 N \text{ bps} \quad (4.7)$$

Where N is the CSK order, if we use two color states, the bit rate is 30 bps, **4-CSK is 60 bps**, **8-CSK is 90 bps** and **10-CSK is 99 bps**.

4.5 Multi-Pixel VLC

So far, the main focus has been establishing a practical VLC link for single-pixel LC under a color-based modulation. Compared to using black-white states, the single-pixel indicates a logarithmic gain in data rates. The grand goal, however, is to increase the data rate by increasing the number of pixels. It produces multiple parallel pathways, and since the camera has a wide angle [5], the frames can store changes from multiple pixels simultaneously. In this manner, the channel capacity increases in linear folds, and if we combine with the passive-CSK at every LC-pixel, we get the following data rate:

$$B_M = M \cdot B \text{ bps} \quad (4.8)$$

B_M is the net data rate of the M -pixel system. To demonstrate the viability of our passive link, we utilize 4 pixels as modulators. The achievable data rate is thus 396 bps. Here, we assign an independent data stream for each

pixel, the pixel then converts them to a stream of CSK-modulated colors. This would require establishing a communication protocol design for our passive-VLC system.

4.6 Packet Protocol Design

Once the data bits are converted to polarized light masquerading as color symbols, we design a protocol that encapsulates and transmits the symbols as packets. The transmission format is depicted in Figure 4.9. Between every data packet, an inter packet gap between the consecutive packets is inserted so that the camera can have some time to automatically adjust it's capturing settings in case there are abrupt changes in the lighting conditions or brightness.

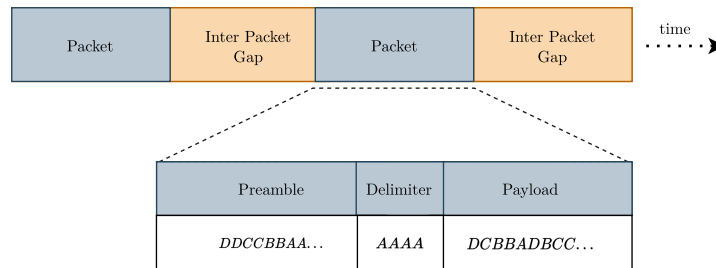


Figure 4.9: **Packet Format in a 4-CSK packet transmitted by a single pixel**

Each packet consists of a preamble, a delimiter, and a payload. The packet size and it's constituents are fixed so that it can be easier to receive and troubleshoot. We will discuss them in detail as follows:

- **Preamble:** The preamble is the first stage of the data packet. It stores a known sequence of symbols required for the decoding training algorithm. Each packet's preamble is repeatedly transmitted three times to provide robust data against variations in the ambient channel. The preamble is also designed for packet detection and synchronization. The first bit or symbol of the preamble is the bit that is maximally separated from packet gap; this way, we can identify the start of the packet with this peak. We shall discuss in detail the utilization of the preamble in the subsequent chapter.
- **Delimiter:** It consists of 4 known continuous symbols that are used for detecting the start of the payload. Without a delimiter to separate the preamble from the payload, and in the presence of noise, the receiver would have difficulty synchronizing.
- **Payload:** The payload segment contains the actual message string that is transmitted, and these data are stored in a CSK encoded format. The size of the payload is roughly 40 percent of the overall size of the network packet.

The structure of the packet is depicted in Figure 4.9. For 4-CSK modulation-based transfer, we transmit 48 symbols of preamble, and four delimiter symbols, and 40 payload symbols. In total, the entire packet size contains 92 symbols.

Chapter 5

Demodulation

As explained in the previous chapter, the LC modulators transmit CSK-modulated signals over the optical link. This chapter explains the process of collecting this modulated polarized light at the camera receiver. After collection, we explain how the system recovers the information signals from the carrier data. We divide the explanation into two parts: **frame extraction**, and **decoding**.

In the extraction stage, the initial step involves capturing the transmission as video. After recording, it is initially processed to detect the location of LCs within the video frames. Object detection methods are utilized to obtain detected boundaries and extract color data at LC stacks. This process is repeated for all frames to extract image data as color intensity versus frames. This down-sampled image data is subsequently stored offline across separate RGB channels. A flowchart depicting this process is presented in Figure 5.1.

Within the decoding stage, our focus shifts towards extracting packets from the stored color-versus-frame number data through signal processing methods on the PC. This process aims to detect packets accurately and interpret transmitted signals with a decoding algorithm. In the presence of communication channel noise, such as attenuation, dispersion, and ambient light, the transmitted signal is often distorted. To mitigate noise, known symbols are transmitted with the packet information. They provide a reference intensity for the message signals. Our work details the training and feature extraction of each known symbol using the *k-means* clustering algorithm. We discuss the frame-to-symbol synchronization, followed by usage of trained data to predict the payload. This synchronization maps the payload intensities across the frames to the intended transmitted symbols, ensuring the correct decoding of the sampled data at the correct time.

5.1 Capture and Extraction

In the context of a communication system, the camera sensor is designed as multiple receiving antennas where each antenna receives data in either of 3 color values: R, G, or B. For a multi-pixel transmission, we consider each LC stack to be a transmitter that emits polarized color beams and establishes a parallel pathway with the receiver. During this process, the antennas receive data from all the stacks simultaneously; this data is converged and translated into color

pixels based on the RGB color model [2]. The resultant image is a 2D grid representation of pixels, with each pixel represented as a vector (C_p), and each constituent intensity ranges from 0-255. In order to capture the entire duration of transmission, it was necessary to record it as a video. Video recording can be viewed as a sequence of frames that are captured at periodic intervals determined by the frame rate (fps). As explained in the modulation chapter, the optimal frame rate can capture the most signal changes while adhering to the sampling theorem. In most modern-day smartphones, the typical maximum recording rate is at slow-motion mode, which enables the recording of videos at 120 fps ([32]).

In addition to channel-induced effects on SNR, the camera’s sensor also affects the quality of the light signal it perceives. The primary camera settings affecting the sensor perception are the *focus* and the *exposure time*. If the focus is not correctly calibrated, abrupt brightness changes will make the captured color pixels appear blurry. The length of time each frame is sampled before transitioning to the next frame is called the frame duration. It is the inverse of the frame rate and is typically 8.33 ms. During this duration, the CMOS sensor is exposed to incoming light for a short period to prevent saturation, which is referred to as the exposure time. The exposure time can vary from 1/500 to 1/2000 seconds depending on the illumination conditions in the environment and can significantly impact the received intensities [5]. If the exposure time is too brief, the camera can capture more frames per second, leading to a higher frame rate and vice versa. The camera software is designed to maintain a consistent frame rate by adjusting the exposure time. However, inconsistencies can still arise, leading to the loss of frames or the capture of additional transmitted frames [25]. Our synchronization mechanism is designed to account for these inconsistencies.

The smartphone camera is set at a fixed focus setting and a frame rate of 120 fps. The recorded video is then transferred for frame processing and signal storage. This is discussed in the next section.

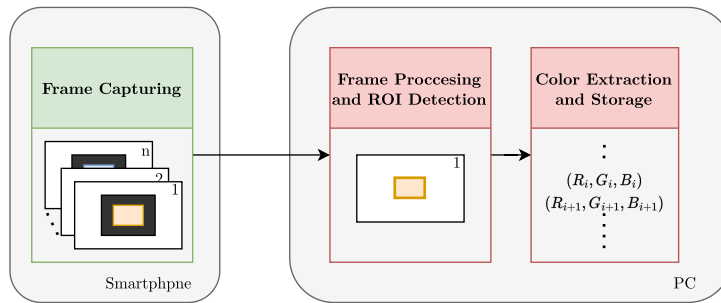


Figure 5.1: **Block diagram detection and extraction**

5.1.1 Detection of ROI

The first step in obtaining the LC’s color information from the video output involves detecting its location or *Region of Interest* (ROI). It is achieved by data processing from the first ten frames. Data loss is not a concern for the initial frames as the transmission remains idle for a brief period, allowing the receiver to

locate the modulators. After that, the data within the detected ROI coordinates are gathered. The exact coordinates are used to repeat the extraction for the remaining video frames. This approach reduces the computational time and processing burden required for locating the ROI. OpenCV [26] object detection functions were employed for this purpose. The following points outline the process:

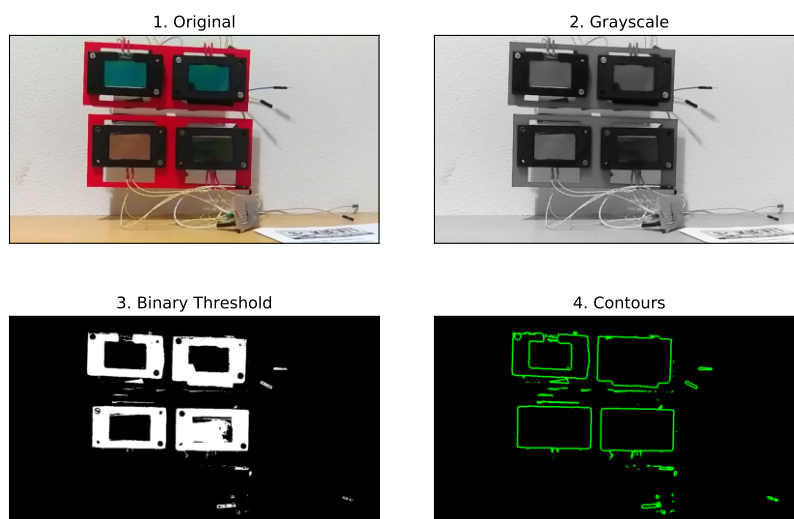


Figure 5.2: First part in the initial Frame Processing

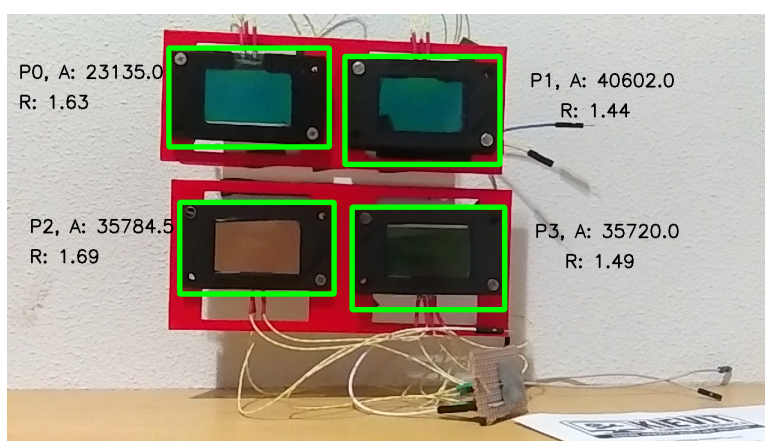


Figure 5.3: Detected Contours around the LC border, with the LC-pixel index, area (A) and aspect ratio (R) displayed as text



Figure 5.4: **Region of Interest within the bounding box for an LC**

- To distinguish the desired foreground objects from the background, we first convert the color image to extract the L (luminance) component from the *Lab* color space [6]. This color space is preferred since it is less sensitive to lighting variations. Next, we apply a threshold to the L component to generate a binary representation, where each pixel is assigned either black or white based on its intensity value. Pixels below the threshold (at value 40) are assigned 0, while those greater than the threshold are assigned 255. The binary image obtained is then subjected to the OpenCV implementation of the *Ramer–Douglas–Peucker* algorithm [9], which identifies the boundaries of foreground objects. These boundaries are commonly referred to as contours. The operation is illustrated in stages 1-4 in Figure 5.2.
- The next step in the process involved determining the boundaries of the transmitter object using its contours. The contours are simplified to simple geometric shapes using the *approxPolyDP()* function. The rectangular shapes were filtered out of these patterns because that is the shape of the Liquid Crystal. We then identified the rectangles that fell within specific area and ratio ranges of the LCs and covered between 10 to 60 % of the image while maintaining an aspect ratio between 1.3 and 1.7. The resulting rectangle coordinates are known as the bounding boxes around the frame of an LC, and the box for each LC region is illustrated in Figure 5.3. Next, we utilized the Linear Indexing method to number the LCs. In this case, we use the top left corner of the image as the reference point. With this, we sort the boxes into rows and columns and assign them numbers as depicted in Figure 5.3.
- After getting the bounding boxes, the next stage is extracting the relevant features of the LC's transmission within the bounding boxes. This involves cropping the box to obtain a subset of the pixels, that is, the region of interest. This cropping avoids pixels in the boundary or the frame. Within this ROI, the overall color is represented by the mean of ROI rather than using individual pixel values. It reduces the amount of data to be stored for post-processing. The mean indicates the color intensity seen from the transmitter and is denoted as a 3-dimensional color vector.

The extracted pixel mean from all succeeding frames is saved as a CSV file consisting of a sequence of RGB vectors. Next, the decoding algorithm processes this data offline, which we detail below.

5.2 Decoding

5.2.1 Decoding Algorithm Flow

Since the data is transmitted as packets, which we illustrate in Figure 5.5, the first step is to detect the packets within the extracted color-frame data. However, this would require synchronizing the receiver algorithm with the packet start, and this is marked by the signal edges at the preamble. We explain this process in the packet detection part in subsection 5.2.2.

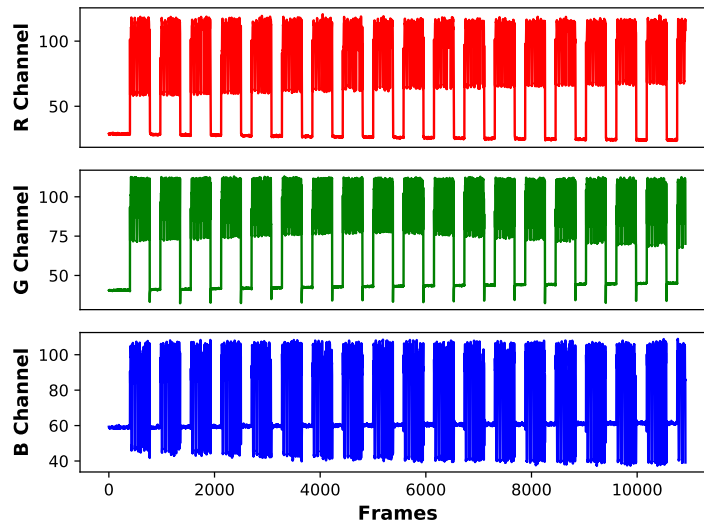


Figure 5.5: **Intensity vs Frame number extracted from video across color channels**

During the packet processing step, we aim to map the payload message back to the originally transmitted data. That requires the decoding algorithm to use the reference data from the preamble. The reference data is essential in every packet because the same symbol can have a different intensity in a different packet. Moreover, the algorithm needs to compensate for noisy channel effects as they affect the signal intensities of the packet. Typically, an equalization method is used for this purpose; for instance, it was employed in RetroI2V [40]. However, it required determining a channel model with complex channel parameters of the optical link. Instead, we employ a machine-learning approach that estimates the SNR, that is, the contrast of the symbols. This approach is a clustering algorithm known as *K-means* that analyzes the received signal from the preamble and extracts features. It does so by making clusters around similar patterns. These trained clusters contain reference color vectors for each symbol which are then employed for predicting message data. However, to

avoid skewing the clustering process, we filter the outlier points using numerical gradients. The clustering stage is detailed in subsection 5.2.3.

During the payload prediction stage, the receiver must synchronize with transmitted data. It ensures that the transmitted data is sampled at the correct instant and can be decoded correctly. For this purpose, we leverage the symbol transitions as instances where we know the symbols have begun or ended. Additionally, the transition detection will facilitate the extraction of stable data values from payload signals. This is done using the rate of change in signal. We apply K-means predictions to decipher our stable payload data, and map the symbols back to binary bits through quantization. The entire flow for this stage is discussed in subsection 5.2.4.

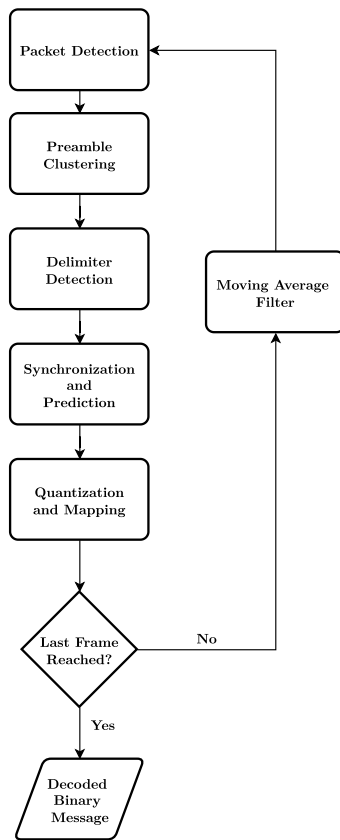


Figure 5.6: Demodulation Algorithm Pipeline

5.2.2 Packet Detection

During the idle gap duration, as shown in the left plot in Figure 5.7, the channel and sensor-induced noise results in fluctuating output in all color channels. The packet identification algorithm is thus a moving average filter that attends to two tasks: smoothen the signal and find signal patterns to search for the packet start. To effectively search for signal changes, the filter window size is set to be less than the size of the idle gap, that is, we consider the size of 20 frames.

This means that this sliding window averages data of 20 samples for each color channel and stores it as a 3D color vector.

The first symbol of the packet is designed to have a significant Euclidean distance from the value of the idle gap symbol. With this knowledge, the moving filter detects a sudden peak at this signal region. The peak is compared with a predetermined threshold known as the start threshold (T_p). In Figure 5.7, we can see the change in the intensity from the idle to the first instance at the packet. Once the packet is detected, we move the receiver’s attention to deciphering the data segments per the packet protocol.

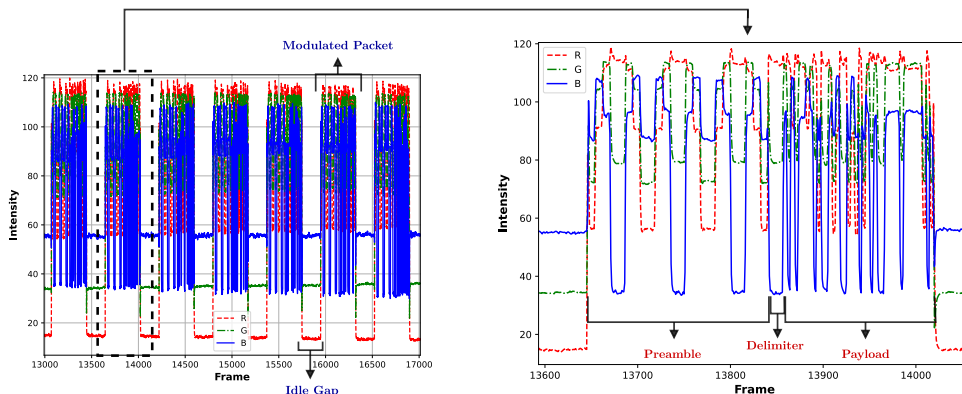


Figure 5.7: Received packets at a magnified view, for a 4-CSK transmission at 30 Symbols per second (Sps).

5.2.3 Preamble and Identifying Clusters

The preamble consists of a pattern of symbols, for instance, in a 4-CSK modulated signal, the sequence is "DDCCBAAAABBCCDD." Our approach is to take the entire set of preamble data and use K-means to identify similar color symbols based on their distances in the RGB space. It partitions them into N clusters, where N is the order of CSK. It is simple and computationally faster than other clustering algorithms [14]. Within that cluster, we obtain a trained pilot symbol that serves as a reference for that symbol cluster.

The size of preamble for K-means training of clusters is based on the following equation:

$$S_p = L_p \cdot f + E \quad (5.1)$$

L_p is the number of preamble symbols transmitted in a packet, and f is the number of frames per symbol. Due to data offsets from camera settings, we cannot pinpoint the frame at which the preamble ends. We assign additional E frames for detecting the end of the preamble. For instance, for a 30 Symbols per second baud rate, f is $120/30 = 4$, and E is five frames. We send 48 preamble symbols per packet; thus, S_p is calculated to have 197 frames.

Filtering Stable Signal

Before applying the training algorithm, we need to filter the outliers in the data, which are the transition points. This is because K-means will make clusters around these outliers points, which can skew the pilot symbol searching calculations. For this purpose, we use the gradient response of the signal to find the transitions.

We explain the method by looking at a single channel response in Figure 5.8; the response is a part of the preamble's intensity vs. frame number. The gradient is calculated with the numerical difference from the previous data point. We get the peaks and troughs corresponding to the transition and take the modulus. Gradient values with more than the threshold value (at value 5) are considered noise and discarded. However, to get a combined gradient response for all the color channels (y_i) and compare with a single gradient threshold (T_g), we use Root Mean Square (RMS) as shown in Equation 5.2. y_{t_i} correspond to transient points, and θ is the first-order numerical difference of a single color channel.

$$\begin{aligned} \theta_{r_i} &= |I_{r_i} - I_{r_{i-1}}|, \quad i \in S_p \\ y_i &= \sqrt{\frac{(\theta_{r_i})^2 + (\theta_{g_i})^2 + (\theta_{b_i})^2}{3}} \\ y_{t_i} &> T_g \end{aligned} \quad (5.2)$$

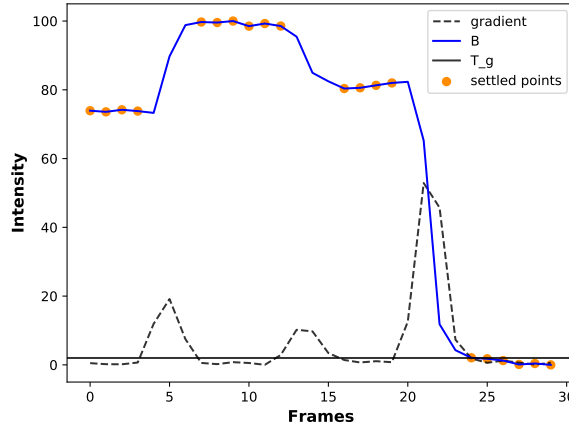


Figure 5.8: Filtering by thresholding the gradient

Training and Labeling

After obtaining the filtered preamble data, we run the K-means works by iteratively partitioning the data into N clusters and adjusting the cluster centers. The algorithm selects k random points as initial cluster centroids. It then assigns each data point to the nearest centroid based on the Euclidean distance metric. Then, the algorithm iteratively updates the centroids by computing the mean of all data points assigned to each cluster. The data points are then reassigned to the closest centroid, and the process is repeated until convergence occurs when

the centroids no longer move. The implementation is employed from *scikit-learn* software library [15]. The centroids thus represent pilot symbols.

As illustrated in Figure 5.9, for transmission over the 4-CSK scheme, we identify four distinct groups that will be represented as spheres. However, the algorithm randomly assigns a symbol label to the cluster. We use a subset of the preamble sequence to assign the correct label. This makes our training algorithm a semi-supervised learning approach. Each preamble symbol is transmitted twice, corresponding to 8 frames of the same symbol. The midpoint intensity in this sequence is taken for labeling. It works even with data offset by one or two frames since it gets more sampled frames with symbol repetition. For example, for symbol 'D,' the intensity of the symbol would be at four frames after the packet start. Then, the cluster centroid closest to this known intensity is designated as 'D.'

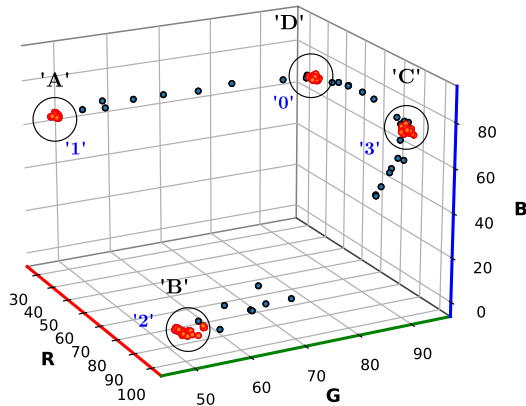


Figure 5.9: Preamble data in color space; the K-means clustered data are orange and within the cluster spheres. The noise are the black points outside the spheres. The k-means assigned random labels are shown in blue, whereas the relabeled symbols are displayed in black

5.2.4 Payload Prediction

Delimiter Detection

The delimiter symbol is designed to be different from the last preamble symbol. For example, the preamble ends with a 'D,' and the delimiter is 'A'. The decoder compares with cluster centers to locate the frame instant at which the intensity corresponds to the last preamble symbol. After which, we synchronize our receiver to the delimiter and preamble. The data prediction begins with the delimiter up to the end of the packet. The size we thus consider is the sum of the delimiter (4 symbols) and payload lengths, and similar to the previous equation, we add extra frames to account for the offset. We can refer to this using the

below equation, where L_m is the payload size. For a 4-CSK transmission, L_m is 40 and E is 5, the size for prediction is thus, $S_m : 4 * (4 + 40) + 5 = 181 \text{ frames}$.

$$S_m = f \cdot (4 + L_m) + E \quad (5.3)$$

Synchronization and Filtering

When the decoder is sampling the payload data, it must align the frames to the sequence of transmitted symbols. This synchronization needs to be done constantly, and one way to achieve this is by employing a sliding window. For example, for four frames per symbol, we have a window of length 4. It would move across the packet, assume the frames-to-symbol correspondence, and decode that symbol. However, data offset of one or more frames will result in a mismatch leading to symbol errors.

Our proposed solution for synchronization is by looking at transitions themselves. Once a transition occurs, the decoder knows the frame/frames at which a symbol ends, and a new one begins. At the same time, identifying transitions can help extract stable data points. This is necessary because the cluster centroids are also trained with stable values, enabling an easier symbol prediction process.

Segregation of transition from the settling data is achieved using the gradient of the data. The method is similar to that discussed in the preamble filtering step. However, we use a different, higher threshold ($=30$) that was determined to account for any symbol transition in the modulation.

The K-means prediction method is employed for each filtered point of the payload segment. It measures the Euclidean distances (formula in Equation 4.4) with each pilot symbol and iteratively identifies the cluster centroid with the minimum distance. This way, the classified symbol has the label of that cluster.

Quantization

After detecting the transition edge, settled points are continuously identified and predicted. The process continues until we reach the next transition peak. These in-between predicted points signify a single symbol or a repetition of the same transmitted symbol. This is because the receiver that satisfies the Nyquist criterion samples in multiple instants across a single symbol. These predicted data points that are classified with the same label are thus quantized to calculate the original number of symbols transmitted. In quantization, the number of predicted symbols is downsampled to the original signal by rounding them using the formula:

$$y_s = \lfloor \nu / f + 0.5 \rfloor \quad (5.4)$$

Where y_s is a positive integer and the number of consecutive times the predicted symbol s was transmitted. ν is the number of times the predicted symbol was detected between two transients, and f is the frames per symbol. For example, in 4-CSK transmission at a rate of 30 Sps, when the predicted symbol 'A' was detected in two consecutive frames, the equation determined that only one symbol 'A' was transmitted for that duration of frames.

Mapping to original bits

We continue the prediction and quantization for continues for the rest of S_m frames until we reach the end of the packet. Downsampled symbols are then mapped to the bits they represent; for instance, 'A' is converted to '00'. The algorithm detects a peak at the last payload symbol and uses a gradient threshold to calculate the frame at which the idle gap begins. After all the transmission packets are decoded, we merge the sequence of the binary bits resulting in the expected sequence of the original message.

In the next section, we evaluate our transmission-reception capabilities in our LC-Camera communication link and analyze if the demodulation can indeed decipher the data with minimal error under different system conditions.

Chapter 6

Testing and Analysis

6.1 Introduction

In order to prove the effectiveness of our modulation-demodulation schemes, we need to test them over a proper hardware setup. Thus, the first part of this chapter details the transmitter and receiver systems. Next, we define the standard parameters and metrics for experimentation. The first set of experiments aims to optimize transmission revolving around the characteristics of a single LC stack. This is conducted through three experiments: transmission throughput, stack size, and the order of CSK. The results determined the optimal system properties that give the least error. With these settings, we conduct experiments to analyze single-pixel systems in different environmental scenarios. The scenarios are the distance with the transmitter, the type of ambient light source, and the tilt of the analyzer. Then, we demonstrate the results of scaling pixels to a 2x2 grid.

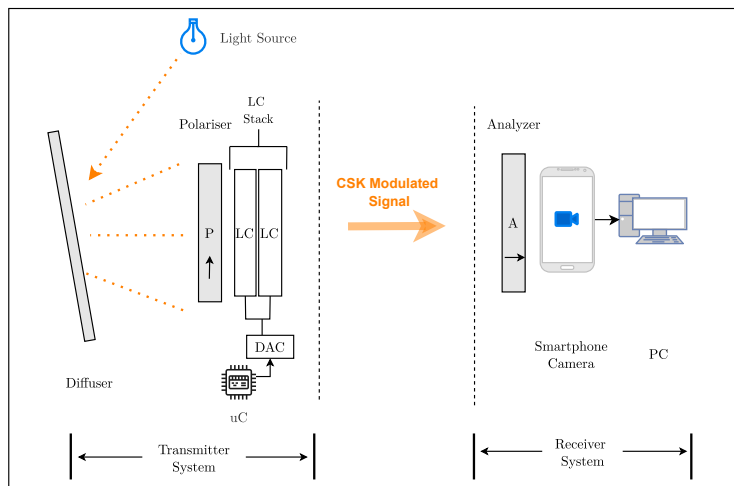


Figure 6.1: System Overview

6.2 Setup

The ambient light communication between LC to camera forms a one-way down-link channel. We can see this in the system configuration illustrated in Figure 6.1. In terms of the transmitter circuitry, there are two configurations: single and a multi pixel. The single LC stack is meant for demonstrating the performance of our communication protocols and methodology. Due to the limited availability of crystals in-hand, the multi pixel transmitter is 2x2 grid of pixels. Through this, we analyze the scalability of the system.

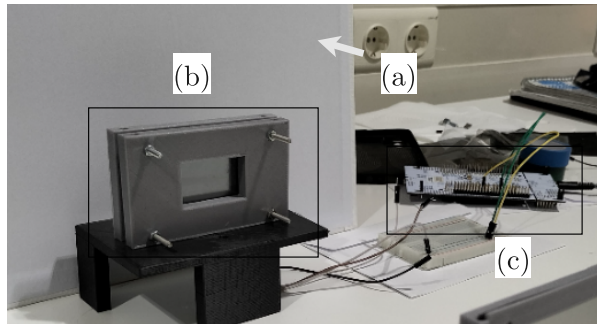


Figure 6.2: **Transmitter Setup**; (a): Diffuser, (b): Enclosed LC Stack, (c): Microcontroller board

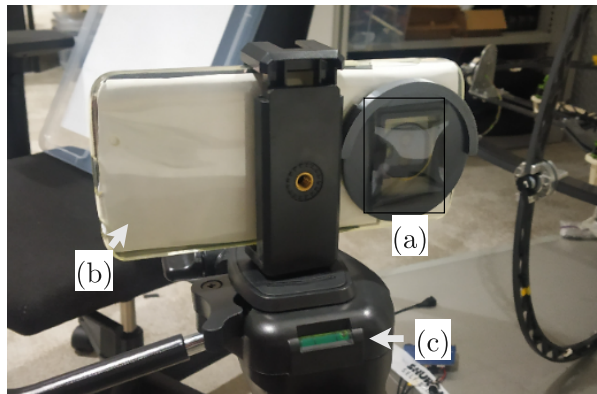


Figure 6.3: **Receiver Setup**, (a): Analyzer, (b): Smartphone, (c): Tripod

6.2.1 Transmitter Design

Since we focus on using Common Off-the-Shelf (COTS) components, we use STM microcontroller *STM32L496 ZG* for digitally generating the transmission symbols. This is achieved through the onboard Digital-to-Analog Converter (DAC). The DAC has an 8-bit resolution and can provide from 0 to 3.3 V, which lies within the operating of the shutters. LC shutter is a 4.2x3.2 cm custom-built TN type [17]. In a stack, all the LCs are connected to a common

DAC pin and ground pin. A 3D-printed enclosure holds the stack and has a larger dimension than the LCs. It creates a border around it so the object detection mechanism can easily distinguish it from the background. The indoor lights are intense resulting in saturated images at the camera. For this reason, we use diffusing panels (as shown in Figure 6.2) to scatter the incoming indoor light before it enters the polarizer.

Multiple-LCs

Due to the limited availability of DAC pins on the Microcontroller (uC) board, we utilized an external DAC module: TLC7528CN. It provides two additional interfaces necessary for the 2x2 pixel grid. We employed a direct addressing approach where the data is transferred by the uC to all the pixels simultaneously. Single pixel setup is shown in Figure 6.2, and the multi-pixel is illustrated in Figure 5.2.

6.2.2 Receiver Design

Since the shutters modulate at a frequency less than 200 Hz, they can cause flickers in the channel link, and to avoid this, we use the late polarization method [3]. In this case, the analyzer is situated before the receiver, as shown in Figure 6.3. The camera is fixed on a tripod to prevent the human hand's shaking from affecting the signal reception. The receiver is a cheap commercial low-end smartphone *Motorola Moto G5*. It supports slow motion mode at a resolution of 1280x720 pixels, which can provide enough perspective to view a multi-pixel grid. For ease of testing, the video is recorded at the camera and transferred to the PC. Then, the PC decoder is responsible for offline post-processing: signal extraction, and execution of the decoding algorithm.

6.3 Evaluation

6.3.1 Metric

Bit Error Rate (BER) metric is used for evaluating the reliability of our communication link. It is defined as the percentage of binary bits that are incorrectly transmitted over a communication channel, relative to the total number of bits transmitted. In VLC systems, the BER is affected by various factors such as ambient light interference, distance, and type of incoming light.

6.3.2 Common Settings

Before transmitting modulated symbols, the transmitter board sends a constant 0 voltage for 5 seconds to allow the receiver to switch on the slow-motion video. The decoder can execute the object detection program during this idle time without missing out on any information packets. The system transmits a standardized amount of around 10,000 bits for evaluation in all scenarios. The bits represent either series of randomized symbols or ASCII strings. For the common setup conditions, and unless specified,

- We test on a single pixel where the stack contains 2 LCs in series. The modulation order is 4-CSK.

Rate (Sym per sec)	BER (%)
10	0
30	0
40	29.81
60	52.65

Table 6.1: **Symbol transmission rate vs Error**

- The polarizer and analyzer are orthogonal to each other. The transmission rate is 30 symbols per sec.
- The illumination are white office ceiling lights at 400 lux. They are located at a height of more than 2 m from the setup.
- The camera’s field of view is along the line of sight. The range of communication is 40 cm.

6.3.3 Modulation Rate

We experiment with different symbol rates to investigate whether the decoding algorithm performs better using sufficient settled points or only with transition points. The receiver’s sampling rate is fixed at 120 fps, which means the system sending rate must be an integer factor of 120. The system is tested with 4-CSK modulation, and the performance results are tabulated in Table 6.1.

As the table indicates, an increase above the 30 Sps mark drastically increases the error. This happens because the decoder captures partial transitions and skips settled points. Also, it samples insufficient settling data making it unreliable at the quantization stage in the decoder. For instance, at 60 Sps, the error is 85 percent for symbols going from 'D' to 'A'. The transition time is 20.8 ms, and the symbol duration is 16.6 ms, causing the error. The optimal rate is thus 30 symbols per second, achieving an acceptable error at the highest throughput.

6.3.4 Stack Size

In this case, we evaluate the optimal number of LCs in a stack for a reliable link. We perform the experiment with a 4-CSK modulation at 30 Sps for a series of 2, 4 and 6 LCs.

Stack Size	BER (%)
2	0.0
3	4.21
4	2.31

Table 6.2: **Performance w.r.t. different number of LCs in series**

As one can notice from the results in Table 6.2, the BER is higher for more than 2 LCs. We note two key points:

We observe a downward trend in the average symbol differences, for stack size 2 LCs it is 90.7, 3 LCs is 88.7, and 4 LCs is 72.3. As we can see in the

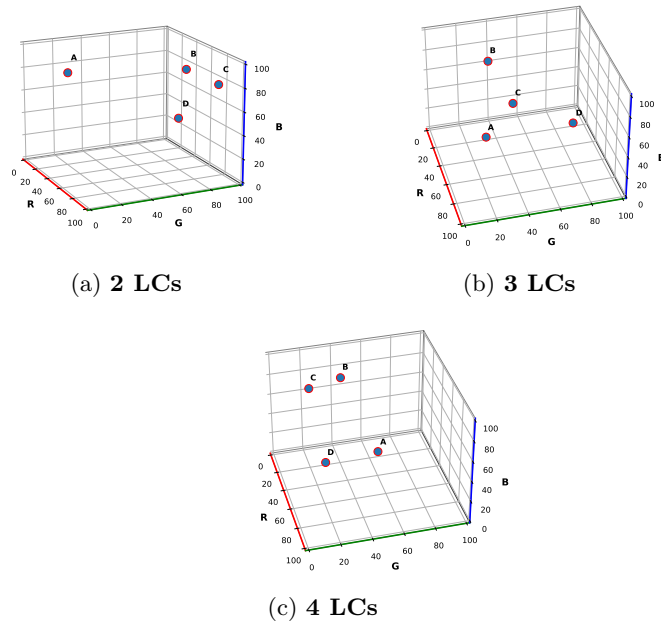


Figure 6.4: **Intensities of cluster centers, with their associated labels**

constellation figures Figure 6.4, the clusters in 4 LCs are present together at the lower end of the color range than far apart symbols in 2 LCs. This results in lower average distances in the former configuration. Also, it can be reasoned that this is due to the reflected light affecting the LC back to the LC, reducing the net intensity of illumination exiting the crystal [10]. However, the contrasts are still higher than the minimum distance threshold. Moreover, the preamble can generate distinct clusters.

The error can be likely attributed to increased response times. Increasing thickness increases the duration of transitions, but we could not establish the reason behind it. To test this hypothesis, we modulate 3 LCs at 20 Sps. The BER drops to 0.55 %. However, more extensive experimentation can be considered for future work to find the transition times for different LC thicknesses. This can be done with transition times experiments for different sizes.

6.3.5 CSK order

This evaluation was aimed to maximize the number of symbols that the modulation scheme can accomplish at a minimal BER. Based on our modulation design limitations, we consider three CSK orders: 4, 8 and 10, transmitting at 30 Sps.

While we achieve zero error rates for the first two CSK types, the system performance in Table 6.3 indicates a spike at 10-CSK. Note that the minimum contrasting distance between some symbols is near the threshold. Considering the channel noise, this caused mispredictions of nearby clusters. For instance, symbols 'A,' 'B', and 'C' are close to each other, this is illustrated in Figure 6.5. It will be an ineffective tradeoff between the increased logarithmic rate for a

much higher BER. Based on the results from the experiments so far, our optimal parameters are two stacked LCs modulating at 4-CSK and 8-CSK schemes at 30 Sps.

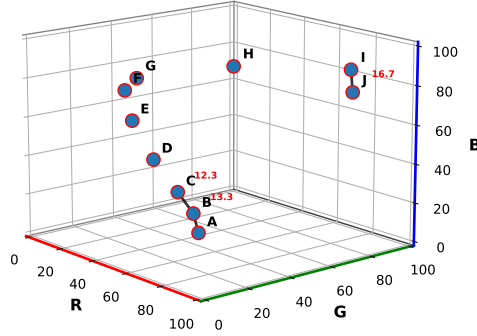


Figure 6.5: **CSK-10 Constellation with close symbol distances marked in red**

CSK Order	BER (%)
4	0
8	0
10	16.6

Table 6.3: **CSK Order**

6.3.6 Distance

Polarized light from the modulator attenuates over the communication distance. Thus, we evaluate the system with distances ranging from 40 cm to 3 m. At every experiment, we zoom the camera view to maintain the visibility of the LC for object detection. The lighting conditions are fixed at 400 lux, and we evaluate for 4-CSK and 8-CSK modulation at 30 Sps.

As observed in Figure 6.6, BER drastically increases for both modulation orders beyond 2 m. It is because the digital zoom decreases the quality of image pixels, thereby worsening the contrast. The unpolarized ambient light of the environment overpowers the incoming polarized light. These factors result in tight symbol clusters, leading to misclassification of payload. The range can be improved using smartphone cameras with much larger zooming capabilities and higher resolutions. On the other hand, the result indicates we achieve a stable link at a maximum throughput of 90 bps upto 1.6 m.

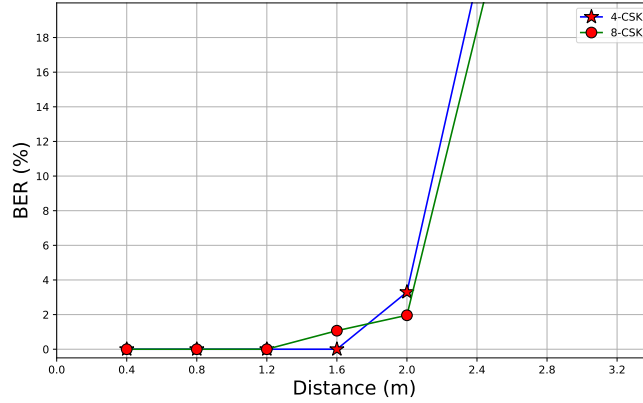


Figure 6.6: **BER plot for the distance between LC and camera**

6.3.7 Lighting Conditions

The system is subjected to different types of illumination incoming the indoor space. We consider two indoor sources: white office lights and a yellow lamp. The lamp is a single source tested in a dark environment and is placed at a distance of less than 1 m. The third source is incoming natural light during typical overcast weather. For non-white sources, The lights are diffused with translucent sheets before interacting at the LC shutters. They are illustrated in Figure 6.10. The BER results are indicated in Figure 6.8.

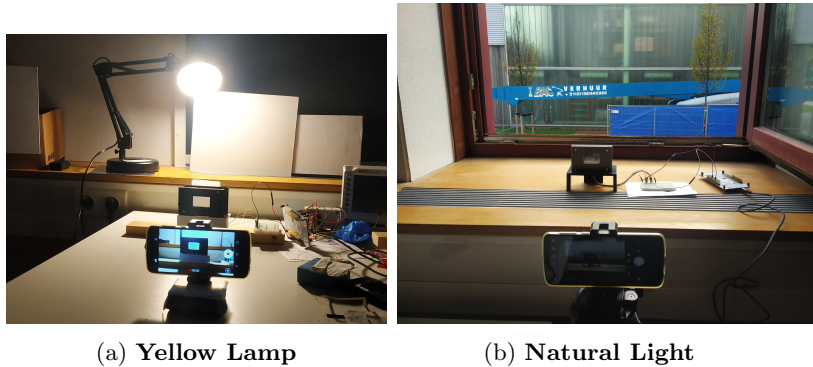


Figure 6.7: **Setup at different lighting scenarios**

While the yellow lamp faces less diffusion compared to other sources, the color intensities are maximum under natural light. This is tabulated in Table 6.4. Nevertheless, the presence of minor fluctuations in the natural light resulted in erroneous packets, which could explain the small error observed. At both 4-CSK and 8-CSK, the system performs the worst under the bulb. We attribute that warm yellow light's spectrum might influence these symbol intensities. The performance can be improved with 4-CSK by choosing a different set of symbols, but it requires investigating symbols with low response times.

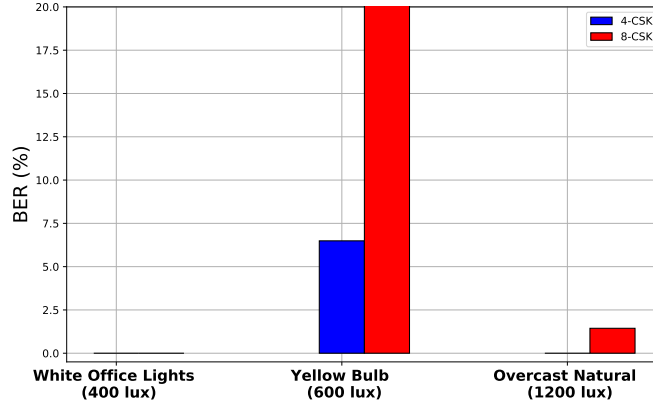


Figure 6.8: Comparison of BER under different sources

Source	Mean Intensity
White Lights	55.4
Yellow Lamp	60.5
Natural Light	78.5

Table 6.4: Mean Intensities of color symbols

6.3.8 Rotation

We investigate the impact of smartphone tilt, that is, the the angle between the polarizer and analyzer. To this end, we test at polarization angles 0° (parallel polarizers condition), 15° and 45° . To simplify the process of detecting bounding boxes, we maintain a stationary camera position while rotating only the analyzer.

When the polarization angles vary, a different color spectrum is generated. It is important to note that the transition times at all angles stay the same because the symbol voltages are unaltered. The BER for 4-CSK stays low ($< 2.8\%$ BER) compared to that in 8-CSK because it is possible to achieve sets of four distinct colors. The color range may not be sufficient to generate eight symbols. The symbol clusters overlap, and cause mislabeling that leads to under-quantization. For instance, the transmitted sequence 'BDAD' is decoded as 'BDD', because the quantization did not receive sufficient 'A' labeled points. This left shift of symbols in the message results in high BER.

6.3.9 Pixel Count

We tested over two configurations for this setup: single pixel and a 2x2 panel of LC stacks. The diffusing element for the multi-pixel is a white-painted wall. The distance is maintained at 40 cm, and the illumination is ceiling light in both cases. The error in the multi-pixel array is the average BER of the individual stacks. The upper half of pixels communicate at error-free links. Conversely, the lower half of the array experiences errors ($< 2\%$ in 4-CSK, $< 3\%$ in 8-CSK). It might be caused by the shadows falling on the wall by the 3D-printed casing

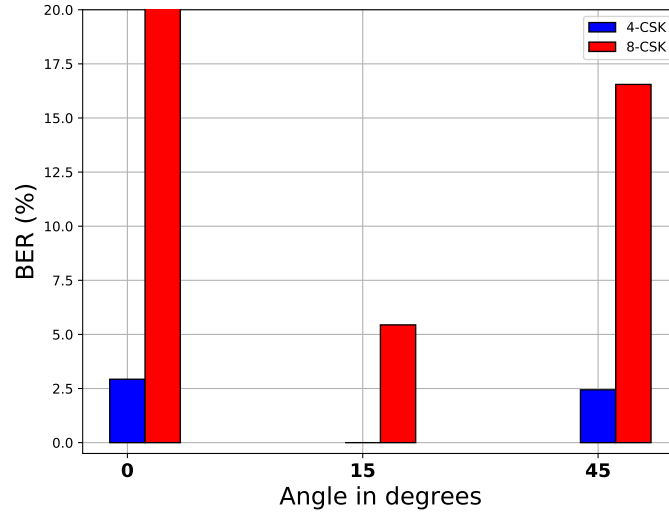
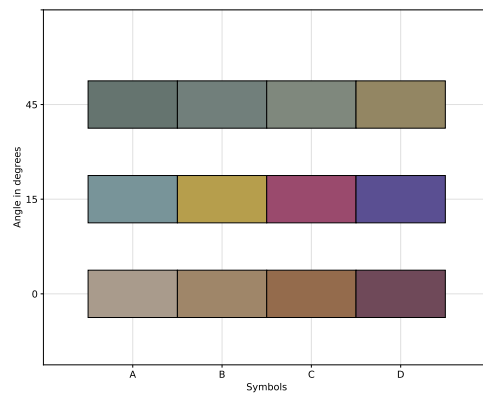


Figure 6.9: **Polarization angle vs BER**

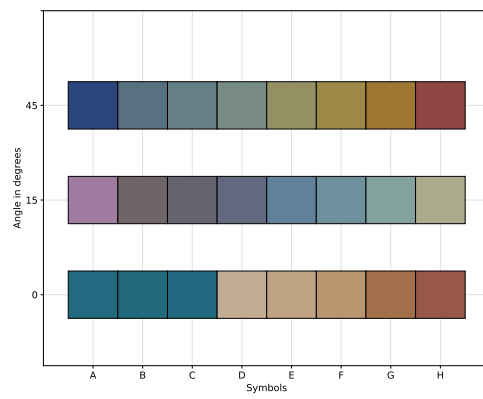
(as shown in Figure 5.3). It causes unwanted variations in the light intensities, making the camera capture the LC stacks with a slightly dull appearance. The optical link can be made more robust with brighter illumination and relocating the setup to reduce the amount of shadow. Additionally, we also can develop a less obtrusive LC panel.

Pixel Count	4-CSK BER (%)	8-CSK BER (%)
Single (1x1)	0.0	0.0
Multiple (2x2)	0.47	1.22

Table 6.5: **Pixel Count vs BER**



(a) 4-CSK



(b) 8-CSK

Figure 6.10: Colors at different orientations

Chapter 7

Conclusion and Future Work

7.1 Conclusion

The aim of this thesis was to enhance the capacity of a passive VLC system, particularly of the LC-to-Camera system. Specifically, the direction of the work was to increase the throughput at a single LC-pixel and achieve linear growth in throughput with a multi-pixel setup. To achieve this, a multi-symbol multi-channel communication link was developed, which demonstrated minimal error.

Our proposed method first explored at using an LC shutter to send multiple symbols. This part was inspired by the recent developments of Chromalux [10], which detailed that birefringent LCs under voltage can generate polarized color beams. We exploited this aspect to develop a color modulation method known as CSK. Unlike most passive-VLC studies [3, 37, 47] that utilized two states, our CSK can encode up to eight symbols of distinct colors, thus increasing the modulation rate by three folds. However, the transition times between the voltages posed a bottleneck. This limited the color design space and resulted in long symbol durations, in the order of tens of ms.

At the receiving end, the camera acquires the data packets containing reference data and the payload. We use a machine learning approach where a clustering-based algorithm extract features from the preamble and produce symbol clusters. Since the receiver is a slow sampling camera and not a fast sampling photodiode, we had the challenge of decoding data with limited sampling points. This was necessary because sampling affects our downsampling algorithm to map points to transmitted symbols. Moreover, even in those points, we had a noise that came as transition points, which posed a challenge in filtering them. Using the rate of the change in signal, we were able to achieve synchronization and filtering of settled data. The trained K-means model then aided in classifying points into symbols.

The second aspect of the study was to increase the pixel count by replicating the single-pixel links. This results in establishing parallel channels with the camera sensor. However, due to the limited availability of shutters and the potential development of complex circuitry, we resorted to a 4-pixel setup. Each stack connects to an individual voltage interface to modulate light symbols.

Our modulation-demodulation methodology was thus evaluated at a single-pixel setup to demonstrate its feasibility.

The optimal configuration for an LC-pixel is at a thickness of 2 LCs and can produce up to 8 distinct colors. Under standard indoor illumination, the setup obtains 90 bps for a maximum range of 1.6 m. Similarly, the rate increases linearly to 360 bps for a 2x2 grid at $< 2\%$ BER. The per pixel performs better than other LC-Camera systems, with a three-fold increase compared to Sunbox's [37] results (30 bps) and a six-fold to PIXEL [47] (at 14 bps). Our scaled system's throughput lags behind Sunbox (10 kbps), although the latter performs at the expense of an expensive LC display, and short range (at 10 cm). Other related studies perform at higher pixel speeds (> 120 bps) due to their use of fast switching modulators and faster sampling speed of photodiodes [16, 45]. Chromalux has a high single-LC rate (> 1 kbps) since it operates on narrow high-contrast transient regions instead of settled states.

7.2 Future Work

The implemented LC-Camera system and the proposed communication methodologies have the potential for improvement in the future. To this end, we outline the following future improvements:

7.2.1 Standalone System

Immediate future work can be in developing a smartphone application that decodes in real-time. This will save the overhead of storing the video for offline processing. However, it may require storing incoming packet data within buffers. Further, a portable transmitter setup with a PCB board can be built that can be placed on a well-lit vertical surface. A solar cell or a battery can connect to power the microcontroller board. For this setup, the protocol can be modeled to include an initiation packet that indicates the start of transmission.

7.2.2 Error Correction

Sunbox sacrificed bit errors to increase transmission speeds beyond the sampling theorem [37]. However, it recovered those losses with Reed-Solomon error correction schemes. A similar proposition can help the LCs to modulate at high symbol rates and potentially recover the misclassified symbols. In addition, error detection like CRC to discard corrupt packets to save processing time.

7.2.3 Decoding Algorithm

In this case, other complex clustering algorithms can be explored, for instance, Hierarchical or Density-based clustering. Also, supervised machine-learning algorithms can be examined, but it might require a substantial number of training samples and necessitate a different protocol format to transmit this type of data to avoid potential mislabeling.

7.2.4 Different LCs

A potential improvement with symbol rates is by examining faster responsive LCs, such as pi-cells [17]. This would involve investigating birefringence response across different thicknesses and response times. In this manner, expanding it to an array of pixels can maximize overall link throughput. However, it can come with hardware challenges, notably the number of connections the COTS board can support with the LCs. If the connections are inadequate, a custom driver circuit may be necessary for data addressing.

7.2.5 High-end Smartphone

Most flagship smartphones offer slow-motion capture at rates exceeding 120 fps. By demodulating at higher frames per symbol, it becomes easier to detect edges and stable regions of the LC. This can yield sufficient points, thereby improving the ability to quantize and detect symbols. Moreover, these cameras can allow for fast-changing shutters as transmitters. It will also offer higher resolution captures, which would operate at longer ranges. We can experiment to investigate the impact of smartphone selection on the BER.

List of Abbreviations

uC Microcontroller	47
BER Bit Error Rate	14
VLC Visible Light Communication	iii
LC Liquid Crystal	iii
OOK On-Off Keying	6
LoS Line-of-sight	12
MIMO multiple-input and multiple-output	13
SIMO single-input and multiple-output	14
SNR Signal-to-Noise Ratio	9
FoV Field-of-View	13
QAM Quadrature amplitude modulation	14
ISI Intersymbol interference	20
CSK Color Shift Keying	3
CSSK Color Sequence Shift Keying	17
FSK Frequency Shift Keying	12

fps frames-per-second	16
RS Reed–Solomon	17
SNR Signal-to-Noise Ratio	9
BCSK Binary Color Shift Keying	16
R Red	21
G Green	21
B Blue	21
RMS Root Mean Square	40
DAC Digital-to-Analog Converter	46
COTS Common Off-the-Shelf	46
Sps Symbols per second	39

Bibliography

- [1] Amazon. Color filter. <https://amzn.eu/d/1kLEb9H>, 2014.
- [2] Vladan Blahnik and Oliver Schindelbeck. Smartphone imaging technology and its applications. *Advanced Optical Technologies*, 10(3):145–232, 2021.
- [3] Rens Bloom, Marco Zúñiga Zamalloa, and Chaitra Pai. Luxlink: creating a wireless link from ambient light. In *Proceedings of the 17th Conference on Embedded Networked Sensor Systems*, pages 166–178, 2019.
- [4] Charles Carver, Shela Wu, Adriana Rogers, Matthew Stafford, N Sertac Artan, and Ziqian Dong. Indoor localization through visible light characterization using front-facing smartphone camera. In *2017 IEEE 14th International Conference on Mobile Ad Hoc and Sensor Systems (MASS)*, pages 575–579. IEEE, 2017.
- [5] Chun-Ling Chan, Hsin-Mu Tsai, and Kate Ching-Ju Lin. Poli: Long-range visible light communications using polarized light intensity modulation. In *Proceedings of the 15th Annual International Conference on mobile systems, applications, and services*, pages 109–120, 2017.
- [6] CUPC CIE. Commission internationale de l’éclairage proceedings, 1931. *Cambridge University, Cambridge*, 1932.
- [7] Giorgio Corbellini, Kaan Aksit, Stefan Schmid, Stefan Mangold, and Thomas R Gross. Connecting networks of toys and smartphones with visible light communication. *IEEE communications magazine*, 52(7):72–78, 2014.
- [8] David JR Cristaldi, Salvatore Pennisi, and Francesco Pulvirenti. *Liquid crystal display drivers: Techniques and circuits*, volume 2. Springer, 2009.
- [9] David H Douglas and Thomas K Peucker. Algorithms for the reduction of the number of points required to represent a digitized line or its caricature. *Cartographica: the international journal for geographic information and geovisualization*, 10(2):112–122, 1973.
- [10] Seyed Keyarash Ghiasi, Marco A Zúñiga Zamalloa, and Koen Langendoen. A principled design for passive light communication. In *Proceedings of the 27th Annual International Conference on Mobile Computing and Networking*, pages 121–133, 2021.

- [11] Yuki Hokazono, Koichi Hasegawa, Yoshiaki Narusue, and Hiroyuki Morikawa. Long-range flicker-free led-to-camera communication using differential color shift keying. In *ICC 2019-2019 IEEE International Conference on Communications (ICC)*, pages 1–7. IEEE, 2019.
- [12] Ke-Ling Hsu, Yu-Chun Wu, Yu-Cheng Chuang, Chi-Wai Chow, Yang Liu, Xin-Lan Liao, Kun-Hsien Lin, and Yi-Yuan Chen. Cmos camera based visible light communication (vlc) using grayscale value distribution and machine learning algorithm. *Optics Express*, 28(2):2427–2432, 2020.
- [13] Pengfei Hu, Parth H Pathak, Huanle Zhang, Zhicheng Yang, and Prasant Mohapatra. High speed led-to-camera communication using color shift keying with flicker mitigation. *IEEE Transactions on Mobile Computing*, 19(7):1603–1617, 2019.
- [14] Manju Kaushik and Bhawana Mathur. Comparative study of k-means and hierarchical clustering techniques. *International Journal of Software & Hardware Research in Engineering*, 2(6):93–98, 2014.
- [15] Kmeans. kmeans.
- [16] Jiangtao Li, Angli Liu, Guobin Shen, Liqun Li, Chao Sun, and Feng Zhao. Retro-vlc: Enabling battery-free duplex visible light communication for mobile and iot applications. In *Proceedings of the 16th International Workshop on Mobile Computing Systems and Applications*, pages 21–26, 2015.
- [17] liquidcrystal technologies. liquidcrystaltechnologies. <http://www.liquidcrystaltechnologies.com/>, 2014.
- [18] Jie Ma, Jing He, Jin Shi, Zhihua Zhou, and Rui Deng. Nonlinear compensation based on k-means clustering algorithm for nyquist pam-4 vlc system. *IEEE Photonics Technology Letters*, 31(12):935–938, 2019.
- [19] Shuai Ma, Jiahui Dai, Songtao Lu, Hang Li, Han Zhang, Chun Du, and Shiyin Li. Signal demodulation with machine learning methods for physical layer visible light communications: Prototype platform, open dataset, and algorithms. *IEEE Access*, 7:30588–30598, 2019.
- [20] markus bauer. calculated_michel_levy_chart. https://github.com/markus-bauer/calculated_Michel_Levy_Chart, 2014.
- [21] Olha Melnyk, Yuriy Garbovskiy, Dario Bueno-Baques, and Anatoliy Glushchenko. Electro-optical switching of dual-frequency nematic liquid crystals: regimes of thin and thick cells. *Crystals*, 9(6):314, 2019.
- [22] Eric Monteiro and Steve Hranilovic. Constellation design for color-shift keying using interior point methods. In *2012 IEEE Globecom Workshops*, pages 1224–1228. IEEE, 2012.
- [23] Eric Monteiro and Steve Hranilovic. Design and implementation of color-shift keying for visible light communications. *Journal of Lightwave Technology*, 32(10):2053–2060, 2014.

- [24] Michael W. Davidson Mortimer Abramowitz. Optical birefringence. <https://www.olympus-lifescience.com/en/microscope-resource/primer/lightandcolor/birefringence/>, 2014.
- [25] Phuoc Nguyen, Nam Tuan Le, and Yeong Min Jang. Challenges issues for occ based android camera 2 api. In *2017 Ninth International Conference on Ubiquitous and Future Networks (ICUFN)*, pages 669–673. IEEE, 2017.
- [26] OpenCV library. opencv. https://docs.opencv.org/3.4/dd/d49/tutorial_py_contour_features.html, 2012.
- [27] Kaveh Pahlavan and Prashant Krishnamurthy. Evolution and impact of wi-fi technology and applications: a historical perspective. *International Journal of Wireless Information Networks*, 28(1):3–19, 2021.
- [28] Hyunha Park, Ikjun Yeom, and Yusung Kim. Watch me if you can: exploiting the nature of light for light-to-camera communications. In *EWSN*, pages 329–334, 2017.
- [29] Pew Research. pewpew.
- [30] Sridhar Rajagopal, Richard D Roberts, and Sang-Kyu Lim. Ieee 802.15.7 visible light communication: modulation schemes and dimming support. *IEEE Communications Magazine*, 50(3):72–82, 2012.
- [31] Muhammad Saadi, L Wattisuttikulij, Yan Zhao, and Paramin Sangwongngam. Visible light communication: opportunities, challenges and channel models. *International Journal of Electronics & Informatics*, 2(1):1–11, 2013.
- [32] Nasir Saeed, Shuaishuai Guo, Ki-Hong Park, Tareq Y Al-Naffouri, and Mohamed-Slim Alouini. Optical camera communications: Survey, use cases, challenges, and future trends. *Physical Communication*, 37:100900, 2019.
- [33] Khaled Shaaban, Md Hosne Mobarok Shamim, and Khadija Abdur-Rouf. Visible light communication for intelligent transportation systems: A review of the latest technologies. *Journal of traffic and transportation engineering (English edition)*, 8(4):483–492, 2021.
- [34] Sihua Shao, Abdallah Khreishah, and Hany Elgala. Pixelated vlc-backscattering for self-charging indoor iot devices. *IEEE Photonics Technology Letters*, 29(2):177–180, 2016.
- [35] Bjørn Eske Sørensen. A revised michel-lévy interference colour chart based on first-principles calculations. *European Journal of Mineralogy*, 25(1):5–10, 2013.
- [36] Michael J Stephen and Joseph P Straley. Physics of liquid crystals. *Reviews of Modern Physics*, 46(4):617, 1974.
- [37] Miguel Chávez Tapia, Talia Xu, Zehang Wu, and Marco Zúñiga Zamalloa. Sunbox: Screen-to-camera communication with ambient light. *Proceedings of the ACM on Interactive, Mobile, Wearable and Ubiquitous Technologies*, 6(2):1–26, 2022.

- [38] The RGB color model mapped to a cube. liquidcrystaltechnologies. `lib.povray.org/searchcollection/index2.php`, 2014.
- [39] videoWindow. videowindow. <https://www.videowindow.eu/>, 2014.
- [40] Purui Wang, Lilei Feng, Guojun Chen, Chenren Xu, Yue Wu, Kenuo Xu, Guobin Shen, Kuntai Du, Gang Huang, and Xuanzhe Liu. Renovating road signs for infrastructure-to-vehicle networking: a visible light backscatter communication and networking approach. In *Proceedings of the 26th Annual International Conference on Mobile Computing and Networking*, pages 1–13, 2020.
- [41] Qing Wang and Marco Zuniga. Passive visible light networks: Taxonomy and opportunities. In *Proceedings of the Workshop on Light Up the IoT*, pages 42–47, 2020.
- [42] Xinyi Wang and Jianhua Shen. Machine learning and its applications in visible light communication based indoor positioning. In *2019 International Conference on High Performance Big Data and Intelligent Systems (HPBD&IS)*, pages 274–277. IEEE, 2019.
- [43] Yang Wang, Evan L. Runnerstrom, and Delia J. Milliron. Switchable materials for smart windows. *Annual Review of Chemical and Biomolecular Engineering*, 7(1):283–304, 2016. PMID: 27023660.
- [44] Arnold Wilkins, Jennifer Veitch, and Brad Lehman. Led lighting flicker and potential health concerns: Ieee standard par1789 update. In *2010 IEEE Energy Conversion Congress and Exposition*, pages 171–178. IEEE, 2010.
- [45] Yue Wu, Purui Wang, Kenuo Xu, Lilei Feng, and Chenren Xu. Turboboosting visible light backscatter communication. In *Proceedings of the Annual conference of the ACM Special Interest Group on Data Communication on the applications, technologies, architectures, and protocols for computer communication*, pages 186–197, 2020.
- [46] Xieyang Xu, Yang Shen, Junrui Yang, Chenren Xu, Guobin Shen, Guojun Chen, and Yunzhe Ni. Passivelc: Enabling practical visible light backscatter communication for battery-free iot applications. In *Proceedings of the 23rd Annual International Conference on Mobile Computing and Networking*, pages 180–192, 2017.
- [47] Zhice Yang, Zeyu Wang, Jiansong Zhang, Chenyu Huang, and Qian Zhang. Wearables can afford: Light-weight indoor positioning with visible light. In *Proceedings of the 13th Annual International Conference on Mobile Systems, Applications, and Services*, pages 317–330, 2015.
- [48] Tai-Cheng Yu, Wei-Ta Huang, Wei-Bin Lee, Chi-Wai Chow, Shu-Wei Chang, and Hao-Chung Kuo. Visible light communication system technology review: Devices, architectures, and applications. *Crystals*, 11(9):1098, 2021.
- [49] Gergely Zachár, Gergely Vakulya, and Gyula Simon. Design of a vlc-based beaconing infrastructure for indoor localization applications. In *2017 IEEE International Instrumentation and Measurement Technology Conference (I2MTC)*, pages 1–6. IEEE, 2017.